

2,4,6-Triaminopyrimidine as a Novel Hinge Binder in a Series of PI3K δ Selective Inhibitors

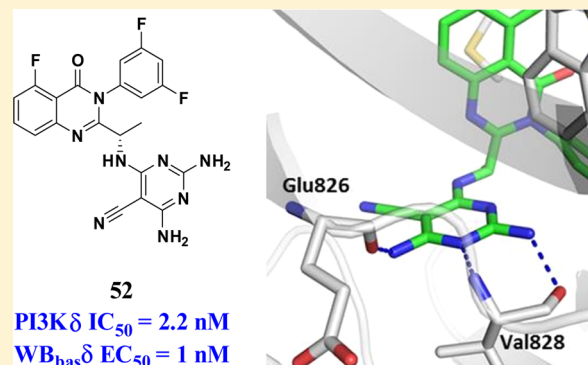
Leena Patel,* Jayaraman Chandrasekhar, Jerry Evarts, Aaron C. Haran, Carmen Ip, Joshua A. Kaplan, Musong Kim, David Koditek, Latesh Lad, Eve-Irene Lepist, Mary E. McGrath, Nikolai Novikov, Stephane Perreault, Kamal D. Puri, John R. Somoza, Bart H. Steiner, Kirk L. Stevens, Joseph Therrien, Jennifer Treiberg, Armando G. Villaseñor, Arthur Yeung, and Gary Phillips

Gilead Sciences, Inc., 199 E Blaine Street, Seattle, Washington 98102, United States

Gilead Sciences, Inc., 333 Lakeside Drive, Foster City, California 94404, United States

S Supporting Information

ABSTRACT: Inhibition of phosphoinositide 3-kinase δ (PI3K δ) is an appealing target for several hematological malignancies and inflammatory diseases. Herein, we describe the discovery and optimization of a series of propeller shaped PI3K δ inhibitors comprising a novel triaminopyrimidine hinge binder. Combinations of electronic and structural strategies were employed to mitigate aldehyde oxidase mediated metabolism. This medicinal chemistry effort culminated in the identification of **52**, a potent and highly selective inhibitor of PI3K δ that demonstrates efficacy in a rat model of arthritis.



■ INTRODUCTION

Phosphoinositide 3-kinase δ (PI3K δ) is critical to the etiology of a number of diseases involving B-cell function.¹ Activation at the cell surface results in PI3K δ catalyzing the intracellular phosphorylation of phosphatidylinositol 4,5-bisphosphate (PIP2) to the second messenger phosphatidylinositol 3,4,5-trisphosphate (PIP3). PIP3 recruits cytosolic signaling enzymes such as Akt that contain pleckstrin homology (PH) domains to the plasma membrane, triggering cell survival, growth, and metabolism.²

PI3K δ is predominantly expressed in hematopoietic cells,³ and inhibition of PI3K δ has been shown to be beneficial for the treatment of hematological malignancies where the PI3K/Akt pathway is hyperactive.⁴

Aberrant signaling in B-cells is also found in a number of inflammatory diseases. PI3K δ is highly expressed in rheumatoid arthritis (RA) synovium,⁵ and inhibition of PI3K δ can reduce both B-cell and T-cell production of inflammatory cytokines that may ameliorate the production of autoantibodies. In models of RA, PI3K δ inhibitors have demonstrated efficacy with respect to inflammation⁶ and reduced bone and cartilage erosion. In allergic asthma, PI3K δ has been shown to be overactive in mast cells,⁷ neutrophils,⁸ T-cells,⁹ eosinophils, and B-cells.

Zydelig (idelalisib), previously called GS-1101 or CAL-101 (**1**) (Figure 1a), is a first-in-class, oral, potent, and selective inhibitor of PI3K δ . Zydelig is dosed twice daily and is approved for use in patients with relapsed chronic lymphocytic leukemia

(CLL), follicular lymphoma (FL), and small lymphocytic lymphoma (SLL).¹⁰

As revealed by the crystal structure (Figure 1b), idelalisib (**1**) binds to the ATP site of the p110 δ catalytic subunit of PI3K δ with the purine forming two hydrogen bonds with hinge residues Val828 and Glu826.¹⁰ The fluoroquinazolinone ring assumes a perpendicular conformation to the hinge binder and is embedded in a specificity pocket between Trp760 and Met752 that is closed in the apo structure of the enzyme.¹¹ The phenyl ring lies perpendicular to the quinazolinone and protrudes out of the ATP-binding pocket into an area known as hydrophobic region II (H2). The improved PI3K δ selectivity of propeller shaped compounds such as idelalisib is presumably due to a lower energy requirement by PI3K δ for the formation of the specificity pocket relative to the PI3K α , PI3K β , and PI3K γ isoforms.^{11b} This previously described binding mode^{11a} is also adopted by several compounds that have been evaluated in clinical studies (Figure 2). Duvelisib, a δ -weighted δ/γ inhibitor, has demonstrated efficacy in B-cell and T-cell lymphomas.¹² AMG-319¹³ and TGR-1202 also inhibit the PI3K δ isoform and have been tested in phase I clinical trials in CLL and non-Hodgkin lymphoma (NHL) patients.¹⁴

In this manuscript, we describe our efforts toward identifying potent, highly selective, and metabolically stable PI3K δ inhibitors, suitable for the treatment of hematological

Received: February 9, 2016

Published: March 16, 2016

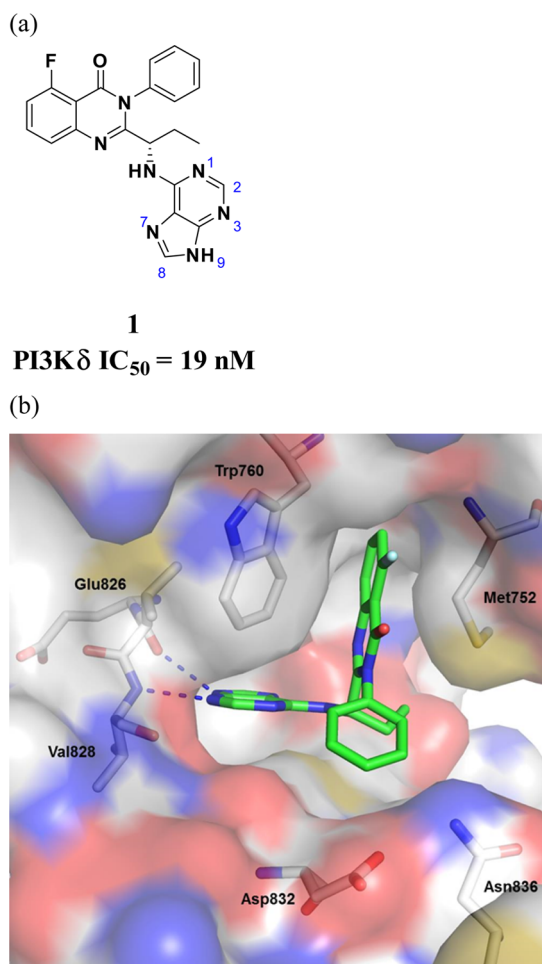


Figure 1. (a) Structure of idelalisib¹⁰ (**1**). (b) 2.4 Å X-ray crystal structure of **1** bound in the PI3K δ ATP-binding site (PDB code 4XE0). Idelalisib (**1**) binds in a propeller shape with the quinazolinone ring occupying an induced specificity pocket formed by Trp760 and Met752. The N3 of the purine hinge binder interacts with the backbone NH of Val828, while the N9 forms short contacts with the backbone carbonyl of Glu826. Blue dashed lines show hydrogen bond contacts between the inhibitor and protein. The Asn836 and Asp832 residues differ among the PI3K isoforms. For clarity, all other residues have been removed.

malignancies and/or inflammatory diseases at a low, once-daily oral dose.

CHEMISTRY

General Synthetic Route to Novel Quinazolinone Compounds. Analogs were synthesized following the general synthetic route shown in Scheme 1.¹⁵ The quinazolinone core **6** was constructed via a one-pot, two-step dehydrative cyclization. Oxazinone intermediate **4** was prepared by treatment of anthranilic acid **2**, with protected amino acid **3** in the presence of diphenyl phosphite and pyridine. Subsequent addition of aniline **5** to the reaction mixture resulted in the formation of the quinazolinone core **6**. Deprotection of **6** with TFA afforded the primary amine intermediate **7** in high yield. Incorporation of the hinge binder motif was attained by nucleophilic displacement of substituted haloheterocycles **8** in the presence of Hünig's base at high temperatures, either thermally or under microwave irradiation.

Preparation of Acetylene-Containing Compounds. An alternative series of pyrimidines targeting the affinity pocket was synthesized according to the sequence described in Scheme 2. Ethynyltrimethylsilane was functionalized via a Sonagashira coupling with the corresponding aryl or heteroaryl bromide **10**. Subsequent deprotection of the silyl protected alkynes afforded compounds of the corresponding terminal alkyne **11**. The synthesis was concluded through a second Sonagashira coupling of **11** with intermediate **12** (synthesized according to the procedure described in Scheme 1) to afford final compounds of the general structure **13** in good yields.

RESULTS AND DISCUSSION

To achieve our goal, we set ourselves a target profile of selectivity greater than 150-fold for PI3K δ over PI3K α , PI3K β , and PI3K γ . This would allow EC₉₀ coverage of PI3K δ at trough concentrations without compromising isoform selectivity. Additionally, a low in vitro human predicted clearance of 0.2 L/h/kg or less was desired for a once-daily dosing regimen. Compound **14** (Table 1) served as an attractive starting point due to its PI3K δ biochemical potency (PI3K δ IC₅₀ = 1 nM). In an effort to optimize metabolic stability we first focused on replacing the purine ring which is the primary site of metabolism for **1**.¹⁶ We designed compound **15** to retain the N3 pyrimidine nitrogen and the 4-amino moiety, both of which were believed to be essential for potency. Unfortunately, this structural modification led to a 100-fold loss in PI3K δ potency relative to compound **14**. The loss in potency may be due to removal of the N7 of the purine ring, which participates in a water-mediated hydrogen bonding network between the quinazolinone ring and the protein.¹⁰ Removal of the 4-amino group (**16**) resulted in an additional loss of potency,

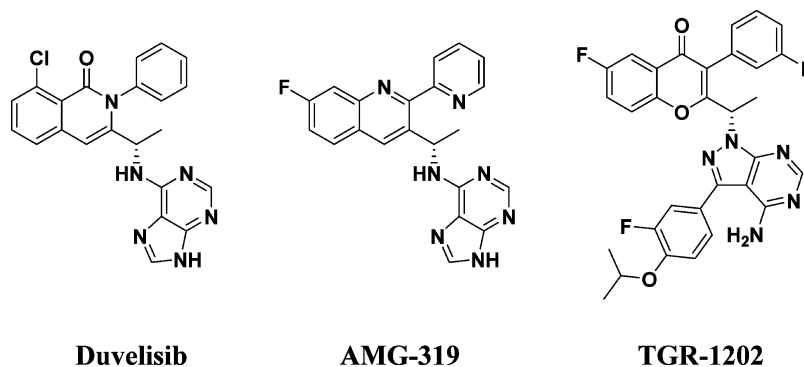
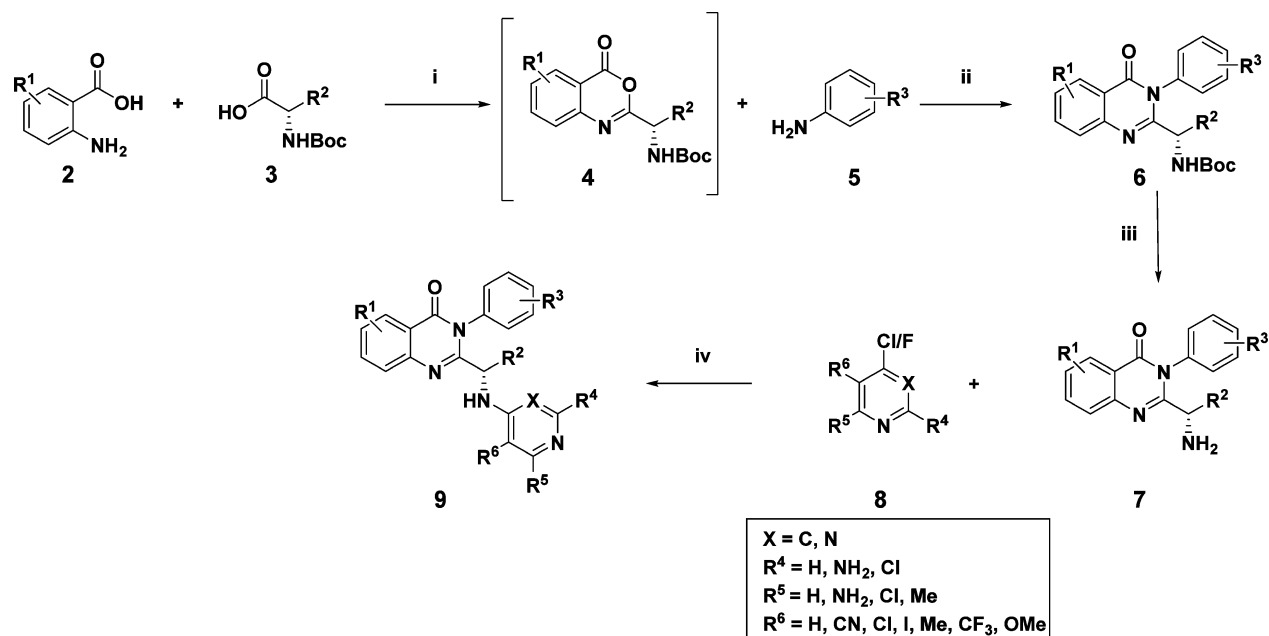
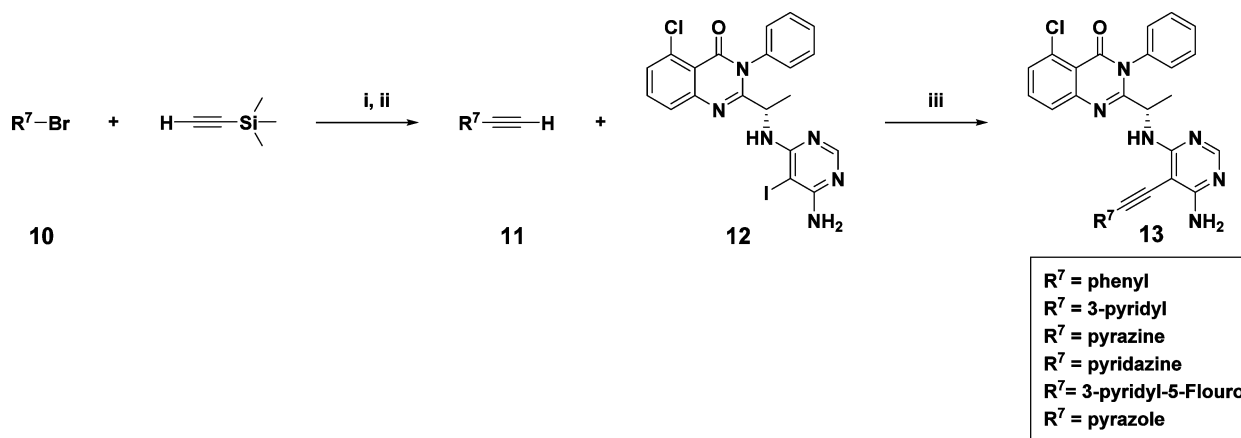


Figure 2. PI3K δ inhibitors in clinical trials.

Scheme 1^a

^aReagents and conditions: (i) pyridine, HOP(OPh)₂, 50 °C, 2 h, 100%; (ii) 50 °C 3–12 h, 50–100%; (iii) CF₃COOH, CH₂Cl₂, rt, 0.5–4 h, 80–100%; (iv) *i*-Pr₂NEt, IPA, 120 °C, microwave or thermal, 8–14 h, 30–95%.

Scheme 2^a

^aReagents and conditions: (i) Pd(PPh₃)₂Cl₂, CuI, Et₃N, toluene, 80 °C, 3 h, 65–80%; (ii) TBAF, THF; (iii) Pd(PPh₃)₂Cl₂, CuI, Et₃N, DMF, 90 °C, 3 h, 60–80%.

illustrating the essential nature of each hinge binding component. Incorporation of a 5-cyano group, exemplified by compounds 17 and 18, restored PI3K δ potency with excellent selectivity over the other PI3K isoforms. We synthesized the pyridine analog 19 which exhibited a 75-fold loss in potency, demonstrating the importance of the N1 nitrogen. Finally, the regioisomer of 18, compound 20, resulted in lower potency and diminished selectivity over PI3K γ . Due to its improved potency and selectivity profile, 18 was advanced into drug metabolism and pharmacokinetic (DMPK) evaluation.

The predicted clearance of compound 18 in human liver microsomes (HLM) and rat liver microsomes (RLM) was determined to be 0.1 L/h/kg and 0.2 L/h/kg, respectively. Encouraged by the low predicted clearances, we progressed 18 to in vivo pharmacokinetic evaluation (Table 2). When administered in rats at 0.44 mg/kg intravenously, 18

demonstrated an intermediate in vivo systemic clearance of 1.1 L/h/kg indicating a 5-fold difference between the observed in vivo clearance and the predicted in vitro microsomal clearance. This discrepancy prompted us to assess susceptibility of the electron deficient 5-cyanopyrimidine ring of 18 to aldehyde oxidase (AO) metabolism. Aldehyde oxidase is a molybdenum-containing cytoplasmic enzyme that catalyzes the oxidation of nitrogen-containing heterocycles.¹⁷ Microsomal assays utilize membrane fractions and do not capture clearance by AO.¹⁸ For that reason, the stability of 18 was tested in human hepatocytes (hHeps) with and without raloxifene, a known inhibitor of AO. A much higher predicted clearance of 0.88 L/h/kg in hHeps was determined for 18 relative to the 0.1 L/h/kg measured in the HLM assay. In the presence of raloxifene there was very little turnover of 18 in the hHeps and the predicted clearance was similar to that observed in HLM

Table 1. Optimization of the Purine Hinge Binder

Hinge

Compound	Hinge	Isoform Selectivity ^{a, b}			
		PI3K δ IC ₅₀ ^a nM	α/δ	β/δ	γ/δ
14		1	1200	290	55
15		99	>100	>100	>100
16		1700	>6	>6	>6
17		8	1200	460	370
18		0.4	4600	200	680
19		30	>340	>340	>340
20		2.5	530	170	15

^aAverage of ≥ 1 determination. Run in quadruplicate. ^bDetermined from isoform specific PI3K IC₅₀ values.

Table 2. DMPK Profile of Compound 18

species	clearance (L/h/kg)		V_{ss} (L/kg) ^{b,c,d}	$t_{1/2}$ (h) ^{b,d}
	in vitro ^a	in vivo ^{b,c,d}		
rat	0.2	1.1 \pm 0.57	2.6 \pm 0.97	2.6 \pm 1.7
human	0.1			

^aFrom hepatic microsomes. ^bIntravenous dose of 0.44 mg/kg. ^cVolume of distribution at steady state. **18** was formulated in 5% ethanol, 75% PEG 400, and 20% citrate buffer (pH 3.0) at 0.09 mg/mL and dosed in Sprague–Dawley rats. ^dNumber of animals per dosing route is 3.

(hHeps + raloxifene = 0.09 L/h/kg). Metabolite identification studies revealed the presence of an M + 16 metabolite **21** (PI3K δ IC₅₀ = 1500 nM), which was verified by independent synthesis (Figure 3). The identity of the product and inhibition of metabolism in the presence of raloxifene are consistent with the involvement of AO in the metabolism of **18**.

Despite the high clearance of **18** in hHeps, the favorable potency and selectivity of this compound prompted us to investigate alternative substitutions at the C5-position on the pyrimidine hinge binder. We hoped to alleviate AO metabolism by modulating the electronics of the pyrimidine ring (Table 3). Hydrolysis of the nitrile of **18** yielded the primary amide **22**, which lost potency, but showed markedly improved hepatic stability compared to **18**. However, the stability of **22** improved further upon incubation with raloxifene, indicating the involvement of AO. As anticipated, the trifluoromethylpyrimidine **23** was also a substrate for AO metabolism. We were hopeful that compound **24** would have diminished AO metabolism due to the presence of a methyl group on the pyrimidine ring. Unfortunately, this modification did not impact susceptibility of the hinge binder toward AO. In addition, **24** was much less potent than **18**, presumably due to weaker interactions of the pyrimidine with the hinge residues. Other electron donating groups such as the methoxy

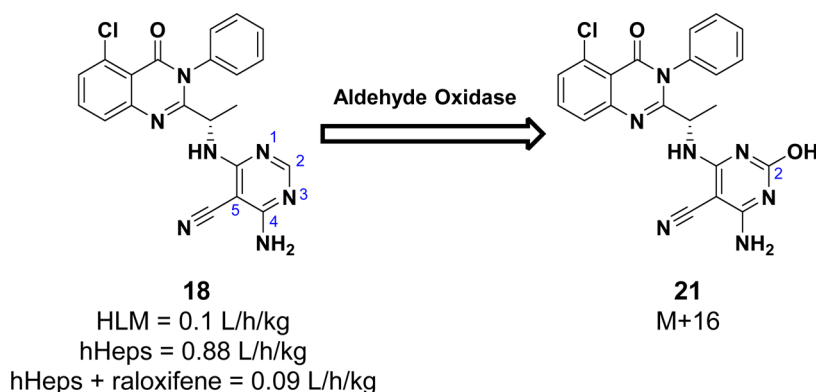


Figure 3. Aldehyde oxidase mediated metabolism of **18** to its M + 16 metabolite **21**.

Table 3. Effect of Modifying the Electronics of the Pyrimidine Hinge Binder

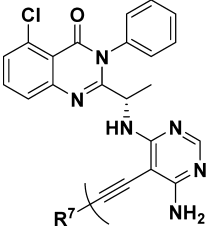
Compound	Hinge	PI3K δ IC ₅₀ ^a	Isoform Selectivity ^{a, b}			hHeps ^c	hHeps + raloxifene ^c
		nM	α/δ	β/δ	γ/δ	L/h/kg	L/h/kg
18		0.4	4600	200	680	0.88	0.09
22		11	860	310	310	0.27	0.08
23		1.8	1200	340	560	0.59	0.12
24		14	700	380	700	0.73	0.25
25		39	>251	>251	>251	ND	ND
26		0.1	9700	490	1900	0.66	ND

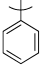
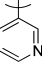
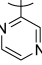
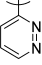
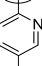
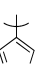
^aAverage of ≥ 1 determination. Run in quadruplicate. ^bDetermined from isoform specific PI3K IC₅₀ values. ^cND: value not determined.

substituent of **25** also resulted in a loss of potency. Terminal acetylene **26** was synthesized to mimic the nitrile of compound **18** and exhibited excellent PI3K δ potency and selectivity. Molecular modeling suggested that elaboration of the terminal acetylene of **26** could allow exploration of the affinity pocket.^{11a}

The affinity pocket is accessed via a narrow channel proximal to the hinge region and is lined with several conserved polar residues. Additional docking studies on a number of analogs suggested that aryl and heteroaryl substituents on the acetylene

Table 4. SAR Results for Acetylene-Containing Compounds



Compound	R ⁷	PI3K δ IC ₅₀ ^a	Isoform Selectivity ^{a, b}		
		nM	α/δ	β/δ	γ/δ
27		0.3	1600	120	320
28		0.5	620	240	100
29		0.4	3200	52	512
30		240	>42	30	>42
31		1.2	2600	330	470
32		0.3	1500	260	230

^aAverage of ≥ 1 determination. Run in quadruplicate. ^bDetermined from isoform specific PI3K IC₅₀ values.

of **26** may be able to interact with these residues through hydrogen bonding and/or π -cation interactions.

To probe the affinity pocket, we prepared analogs **27–32** (Table 4). Phenyl analog **27** exhibited good inhibition of PI3K δ but diminished PI3K β selectivity. Compounds **28** and **29**, although potent, lost selectivity over PI3K γ and PI3K β , respectively. The pyridazine analog **30** suffered considerable potency loss, possibly due to a repulsion between the heterocycle and nearby residues in the affinity pocket. An overall improvement in potency and isoform selectivity was achieved with compounds **31** and **32**. To better understand the potency of the affinity compounds, we examined an X-ray cocrystal of compound **32** bound to PI3K δ (Figure 4). The crystal structure illustrates the formation of two hydrogen bonds between the aminopyrimidine and the hinge residues, Val828 and Glu826. In addition, the pyrazole of **32** forms short contacts with Lys779, Asp911, and Asp787 in the affinity pocket. These supplementary hydrogen bonds help explain the gain in enzyme potency achieved with the acetylene-containing compounds. Hopeful that the significant structural modifications relative to **18** would perturb AO recognition of the hinge binder^{17d,19} we quantified the metabolic fate for **31** in hHeps (\pm raloxifene). Unfortunately, compound **31** exhibited a 4-fold reduction in predicted clearance when incubated with

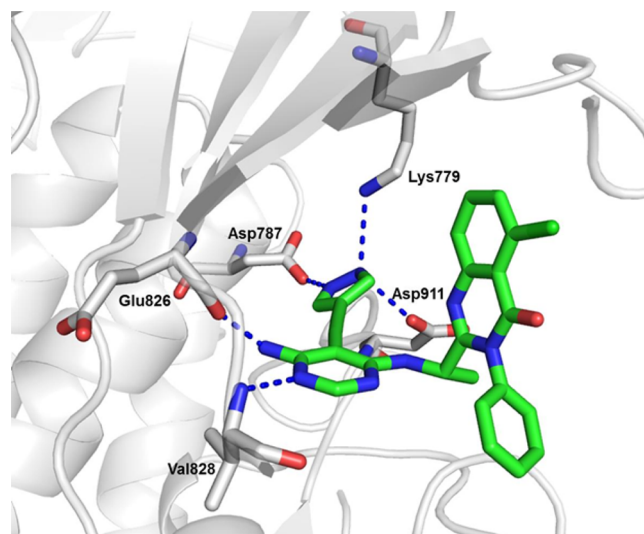


Figure 4. 2.85 Å X-ray crystal structure of **32** bound in the PI3K δ ATP-binding site (PDB accession code 5I6U). In addition to the classic hinge binding interactions, the pyrazole ring forms hydrogen bonds to Lys779, Asp911, and Asp787 in the affinity pocket.

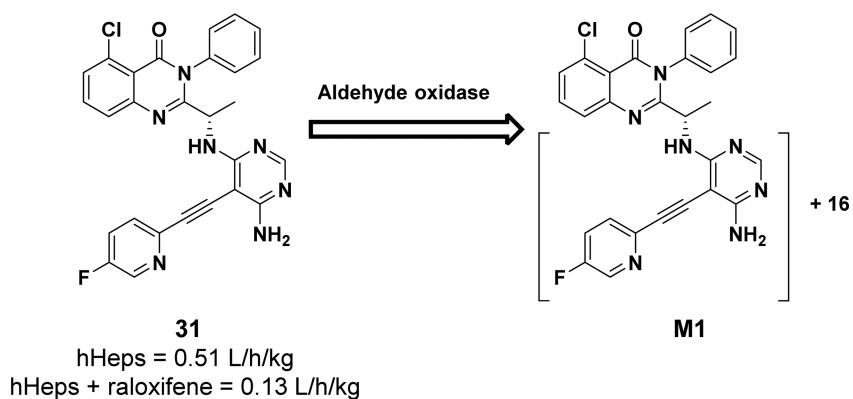


Figure 5. Aldehyde oxidase mediated metabolism of 31 to its metabolite M1.

Table 5. SAR Results for Fully Substituted Pyrimidines

Compound	Hinge	PI3K δ IC ₅₀ ^a nM	Isoform Selectivity ^{a, b}			hHeps L/h/kg	hHeps + raloxifene ^c L/h/kg
			α/δ	β/δ	γ/δ		
18		0.4	4600	200	680	0.88	0.09
33		1.2	1200	70	420	0.50	0.10
34		0.1	2200	80	60	0.21	0.10
35		4.3	720	180	37	0.59	ND
36		0.9	2700	370	200	0.65	ND
37		1.0	530	100	25	0.82	ND
38		0.13	1900	100	40	1.05	ND

^aAverage of ≥ 1 determination. Run in quadruplicate. ^bDetermined from isoform specific PI3K IC₅₀ values. ^cND: value not determined.

raloxifene (0.13 L/h/kg); metabolite identification studies of 31 revealed an M + 16 metabolite M1, implicating AO metabolism (Figure 5). Despite marked improvement in

isoform selectivity of 31 and 32, the involvement of AO in the metabolism of these analogs deterred us from further exploration of acetylene-containing compounds.

Achieving metabolic stability was paramount in our program; electronic and structural modifications of the hinge binder failed to alleviate AO metabolism. Therefore, we decided to focus on an alternative strategy, directed at blocking oxidation of the C2-position on the pyrimidine ring. Deuteration at C2 (**33**) modestly improved predicted clearance in hHeps compared to **18** (Table 5). Subsequent incubation of **33** with raloxifene revealed a 5-fold reduction in hepatic clearance implicating the involvement of AO. Substitution with a primary amine (**34**) afforded high potency and low clearance that was insensitive to the presence of raloxifene. The low predicted hepatic clearance of **34** was attractive but was accompanied by an increase PI3K β and PI3K γ potency. Other blocking groups such as chlorine (**35**) resulted in a loss in potency, a further loss of PI3K γ selectivity, and a higher predicted clearance relative to **34**. The poor metabolic stability is presumably due to an increase in lipophilicity (calculated $\log P = 3.7$ vs 3.0 (**34**)). Similarly, other small substituent changes around the pyrimidine ring (**36–38**) furnished compounds that exhibited high predicted clearances. The 2-amino substituent of **34** demonstrated a unique ability to successfully block AO metabolism at the C2-position while retaining PI3K δ potency. The X-ray cocrystal of **34** bound to PI3K δ reveals the triaminopyrimidine as a three-point hinge binding motif. In addition to a hydrogen bond between the N3 and the backbone NH of Val828, a second hydrogen bond is formed from the N4 to the backbone carbonyl of Glu826. The 2-amino substituent of the triaminopyrimidine supplements the typical N3 and N4 hinge binding features with a third hydrogen bond to the carbonyl of Val828 (Figure 6).

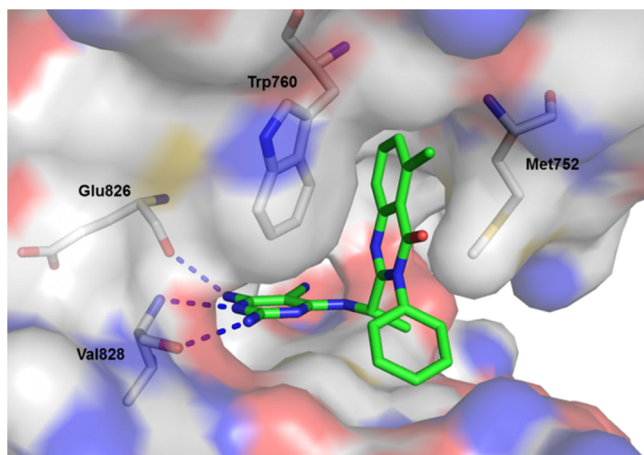


Figure 6. 2.4 Å X-ray crystal structure of **34** in PI3K δ illustrates the triaminopyrimidine establishing hydrogen bonds to the hinge residues, Val828 and Glu826. A third hydrogen bond is accomplished between the N2 component of the triaminopyrimidine hinge binder and the carbonyl of Val828 (PDB accession code 5I4U).

Inspired by the potency and predicted clearance of **34**, we focused our efforts upon improving isoform selectivity. The H2 region of the p110 δ subunit of PI3K δ consists of two residues lining the edge of the pocket that is filled by the phenyl ring. These residues differ among the PI3K isoforms; sequence alignments reveal Asp832/Asn836 in PI3K δ correspond to His/Gln in PI3K α , Glu/Asp in PI3K β , and Thr/Lys in PI3K γ . As a result, the electrostatic and steric environments are significantly different across the isoforms. We hypothesized that small substituents on the phenyl ring could influence isoform

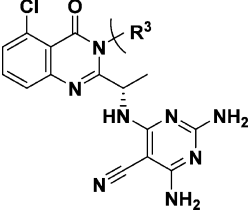
selectivity. The addition of a fluoro substituent on the para position (**39**) resulted in significant loss of isoform selectivity (Table 6). On the other hand, substitutions on the meta position (**40–45**) displayed similar selectivity profiles to that of **34** with respect to PI3K γ . We thought that we may be able to further improve the isoform selectivity of compound **42** by the addition of a second group to the 5-position on the phenyl ring. Bis-nitrile **47** resulted in a considerable loss of PI3K δ potency, possibly due to steric interference between the bulky isophthalonitrile ring and the enzyme. However, we were pleased to see that compounds **46**, **48**, and **49** demonstrated improved isoform selectivity relative to **34**. These experimental results confirmed that small substituents at the 3- and 5-positions on the phenyl ring are well accommodated in PI3K δ .

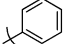
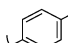
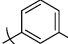
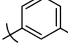
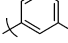
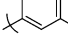
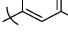
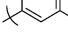
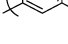
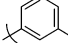
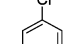

While exploring alternative substitutions on the quinazolinone ring, we found that minor modifications had substantial impact on potency and selectivity. Despite the relatively high clearance of **49** in human hepatocytes (hHeps = 0.81 L/h/kg), we chose to retain the 3,5-difluoroaniline moiety since it afforded an enhanced selectivity profile over the unsubstituted phenyl ring of **34**. Addition of a fluorine atom to the 6-position of the quinazolinone, **50**, resulted in a 5-fold loss in PI3K δ potency and lower δ/γ selectivity (Table 7). Complete removal of substitutions on the quinazolinone core (**51**) afforded a less potent and a more stable compound relative to **49**. The diminished hepatic metabolism of **51** may be due to a decrease in lipophilicity (calculated $\log P = 2.6$ vs 3.3 (**49**)). We subsequently focused upon designing compounds with reduced lipophilicity relative to **49**. The fluorine analogs (**52–54**) were slightly less lipophilic (cLogP = 2.6 (**52–54**)) and offered a balance of potency and selectivity. Additionally, we were pleased to find that both **52** and **53** displayed lower predicted clearances in hHeps in comparison to **49**. We saw a substantial boost in isoform selectivity with the 8-cyano compound (**55**); unfortunately, **55** exhibited a higher clearance in hHeps relative to **52**. We found **52** to offer us a favorable combination of biochemical potency, isoform selectivity, and metabolic stability. Additionally, when tested in a whole blood basophil cellular assay (WB_{bas} δ), analog **52** potently inhibited PI3K δ , with an EC₅₀ of 1 nM. We further assessed **52** using the KinomeScan platform against a panel of 395 nonmutant kinases at a single concentration of 10 μ M. Compound **52** displayed a high degree of kinome selectivity by only binding to other lipid kinases at less than 10% of control.

We next evaluated the PK profile of **52**. When administered in vivo, **52** demonstrated low to intermediate total clearance in rat and dog in comparison to hepatic blood flow in these species, high volumes of distribution, and high oral bioavailability (Table 8). Rat PK for **52** suggested achievable target coverage at trough concentrations with twice-daily administration without compromising PI3K isoform selectivity (Figure 7). Additionally, **52** inhibited ex vivo anti-IgD stimulation of B-cells with EC₅₀ and EC₉₀ values of 11 and 100 nM, respectively, as determined by a rat whole blood assay. Therefore, **52** was dosed to maintain these levels in a rat established collagen-induced arthritis (CIA) model.

This experimental model of polyarthritis has been widely used for preclinical testing of numerous antirheumatic agents.²⁰ In this experiment, female Lewis rats with established CIA were treated twice daily by oral gavage for 7 days starting on the tenth day after collagen treatment, with vehicle or **52** at 0.34, 1.07, 4.6, and 10 mg/kg. Efficacy evaluation was based on reduction in paw swelling (measured by daily ankle caliper

Table 6. Optimization of Phenyl Ring in H2



Compound	R ³	PI3K δ IC ₅₀ ^a	Isoform Selectivity ^{a, b}		
		nM	α/δ	β/δ	γ/δ
34		0.1	2200	80	60
39		2.0	64	4	2
40		0.15	3100	550	90
41		0.45	530	140	70
42		1.9	1700	340	90
43		0.9	1100	330	70
44		3.6	1100	230	57
45		1.6	1400	230	120
46		0.54	1800	190	210
47		150	>68	>68	>68
48		1.5	850	220	220
49		0.47	2600	520	110

^aAverage of ≥ 1 determination. Run in quadruplicate. ^bDetermined from isoform specific PI3K IC₅₀ values.

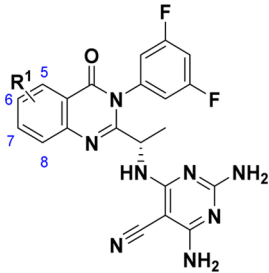
measurements and terminal hind paw weights) and histopathology parameters (amelioration of inflammatory infiltrate, pannus formation, cartilage destruction, and bone resorption). Treatment of animals with established CIA with **52** showed significant and dose-dependent reduction in ankle swelling (Figure 8).

A correlation between plasma concentration of **52** and the degree of target inhibition leading to efficacy was established utilizing a rat whole-blood ex vivo BCR-induced B-cell activation assay. Compound **52** inhibited PI3K δ -mediated B-

cell activation in vivo with an EC₅₀ of 20.5 nM and an EC₉₀ of 100 nM. These values were used to assess the degree of target inhibition at the dose levels tested in the CIA model. Plasma concentrations measured on days 3 and 7 were consistent with maintaining approximately 25%, 50%, 90%, and >90% inhibition of PI3K δ at 0.34, 1.07, 4.6, and 10 mg/kg doses, respectively, at trough levels (Figure 9).

Histopathology showed animals treated with 1.07 mg/kg, targeting EC₅₀ inhibition at trough, had significantly ameliorated ankle inflammation (45% reduction), pannus formation

Table 7. SAR Results for Quinazolinone Ring Modifications



compd	R ¹	PI3K δ IC ₅₀ ^a (nM)	isoform selectivity ^{a,b}			hHeps (L/h/kg)
			α/δ	β/δ	γ/δ	
49	5-Cl	0.47	2600	520	110	0.81
50	5-Cl, 6-F	2.9	780	470	74	0.39
51	H	15	530	290	75	0.17
52	5-F	2.2	1900	650	180	0.34
53	6-F	4.8	600	520	160	0.29
54	8-F	3.5	810	920	130	0.53
55	8-CN	5.9	1700	1200	800	0.5

^aAverage of ≥ 1 determination. Run in quadruplicate. ^bDetermined from isoform specific PI3K IC₅₀ values.

(60%), cartilage damage (50%), bone resorption (63%), and periosteal bone width (52%), as compared to vehicle controls, with ED₅₀ values calculated at approximately 1.5 mg/kg on all disease parameters (Figure 10). Maintaining PI3K δ coverage between EC₅₀ and EC₉₀ over the dosing interval was sufficient to significantly reduce disease scores in this rat established model of RA.

CONCLUSION

In summary, we have optimized a series of potent and highly selective PI3K δ inhibitors. During the course of our research we discovered a novel triaminopyrimidine hinge binder that forms three hydrogen bonds with the protein. We also optimized the phenyl and the quinazolinone regions for potency and isoform selectivity. Compound **52**, although not suitable for once-daily dosing, was identified as a potent and selective inhibitor of PI3K δ with good pharmacokinetic properties. Moreover, **52** demonstrated efficacy in a model of rat CIA with less than complete target coverage over the dosing interval. Further work and additional optimization to achieve a low dose PI3K δ inhibitor suitable for QD administration will be presented in a future publication.

EXPERIMENTAL SECTION

General Procedures. All final compounds were determined to be at least 95% pure by ¹H NMR and LCMS analysis. All commercial reagents and anhydrous solvents were used as provided without

Table 8. DMPK Profile of Compound **52**

species	clearance (L/h/kg)		V _{ss} (L/kg) ^{b,c,f}	b/p ^d	t _{1/2} (h) ^{e,f}	F (%) ^{e,f}
	in vitro ^a	in vivo ^{b,f}				
rat	1.4	0.74 ± 0.04	2.6 ± 0.37	1.4	3.2 ± 0.19	106 ± 24
dog	0.25	0.58 ± 0.16	1.30 ± 0.1	2.6	2.17 ± 0.56	100 ± 40
human	0.34					

^aFrom hepatocytes. ^bIntravenous dose of 1 mg/kg. ^cVolume of distribution at steady state. ^dBlood plasma ratio. ^eOral dose of 5 mg/kg. **52** was formulated in 30% PEG 400 and 70% water for dosing in rats for both iv and po, and 5% ethanol, 55% PEG 400, and 40% citrate buffer at pH 2 (iv) and 15% Captisol (w/v) in water (po) for dosing in dogs. ^fNumber of animals per dosing route is 3.

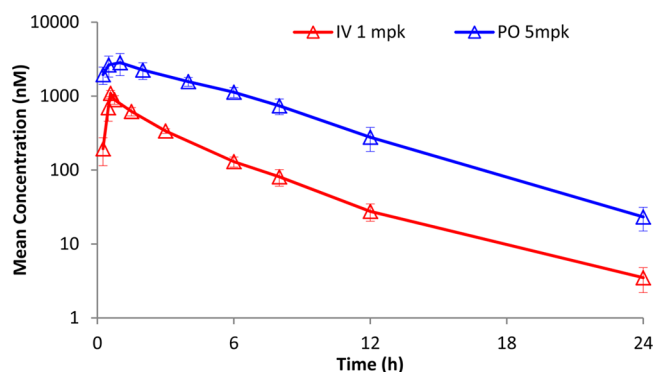


Figure 7. Concentration–time profiles of **52** in plasma following a 30 min intravenous infusion at 1 mg/kg and an oral dose at 5 mg/kg in female Lewis rats (mean ± SD, *n* = 3). The bioavailability of **52** was 106 ± 24%. The C_{max} was 2830 ± 942 nM at 1 h, and AUC_{inf} was 17000 ± 3930 nM·h.

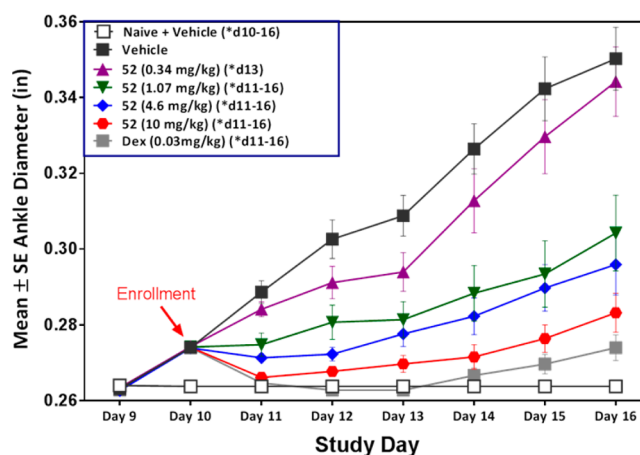


Figure 8. Compound **52** ameliorates ankle swelling in rat established CIA model. Female Lewis rats with CIA were treated, twice daily by oral gavage, for 7 days (study days 10–16) with vehicle, **52** (0.34, 1.07, 4.6, or 10 mg/kg), or the reference compound dexamethasone (0.03 mg/kg). Caliper measurements of right and left ankle diameters were taken every day beginning on day 9 and continuing through day 16: (*) *p* < 0.05 versus arthritis + vehicle.

further purification. Microwave reactions were completed using a benchtop CEM microwave reactor. Flash chromatography was performed using an ISCO Combiflash or a Biotage Isolera purification system with Silicycle prepacked silica gel cartridges. Final compounds were purified by prep HPLC on a Gilson 271 system, with a Phenomenex Kinetex C18 column (250 mm × 30 mm, 100 Å, 5 μm) and a gradient elution of acetonitrile/water with 5–95% for 20 min at a flow rate of 35 mL/min. For all samples 0.1% TFA was added to both eluents. All ¹H NMR spectra were recorded on a Varian 400-MR 400 MHz spectrometer. Proton chemical shifts are reported in parts

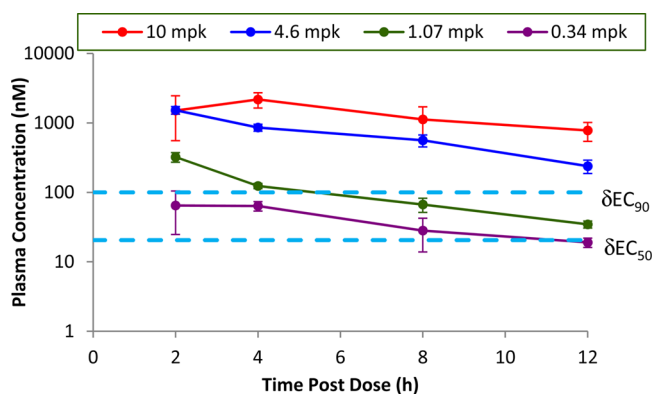


Figure 9. Pharmacokinetic profile of **52** in Lewis rats with established CIA. Blood samples from each dose group animals at indicated time after dosing on days 3 and 7 were analyzed for plasma concentrations of **52**.

per million from an internal standard or residual solvent. The purity of the tested compounds was assessed by an Agilent LCMS. A Silicycle Siliachrom SB C18 column (4.6 mm × 50 mm, 3 μm) was used with a gradient elution of acetonitrile in water, 0–95% for 7 min at a flow rate of 0.9 mL/min with detection at 256 nm. Alternatively, a Chromolith column (50 mm × 2 mm) was used with a gradient elution of acetonitrile in water, 0–95% for 3 min at a flow rate of 1.9 mL/min with detection at 256 nm. For all samples 0.1% TFA was added to both eluents.

(S)-2,4-Diamino-6-((1-(5-chloro-4-oxo-3-phenyl-3,4-dihydroquinazolin-2-yl)ethyl)amino)pyrimidine-5-carbonitrile 2,2,2-Trifluoroacetic Acid Salt (34). **34** was synthesized according to the procedure described in [Scheme 1](#). 2,4-Diamino-6-chloropyrimidine-5-carbonitrile (391 mg, 2.31 mmol) was added to a suspension of (*S*)-2-(1-aminoethyl)-5-chloro-3-phenylquinazolin-4(3*H*)-one 2,2,2-trifluoroacetic acid salt (865 mg, 2.89 mmol) (**7**) and diisopropylethylamine (7.6 mL, 43.3 mmol) in IPA (3 mL). The resultant mixture was heated to 130 °C for 14 h, after which time the reaction was cooled to room temperature. The resultant solid was filtered and purified by HPLC, eluting with 5–95% water/acetonitrile (0.1% v/v trifluoroacetic acid). The appropriate fractions were pooled and lyophilized to afford the title compound as a white solid (575 mg). ¹H NMR (400 MHz, DMSO) δ 7.78 (t, *J* = 8.0 Hz, 1H), 7.63 (dd, *J* = 8.2, 1.2 Hz, 1H), 7.57 (dd, *J* = 7.8, 1.2 Hz, 1H), 7.57–7.45 (m, 5H), 6.79 (d, *J* =

7.0 Hz, 1H), 6.55 (br s, 1H), 6.25 (br s, 1H), 4.72 (dq, *J* = 6.45, 6.45 Hz, 1H), 1.29 (d, *J* = 6.8 Hz, 3H). ES/MS *m/z* 433.1 (M + H)⁺.

(S)-2-(1-Aminoethyl)-5-chloro-3-phenylquinazolin-4(3*H*)-one 2,2,2-Trifluoroacetic Acid Salt. Trifluoroacetic acid (3 mL) was added to a solution of (*S*)-*tert*-butyl 1-(5-chloro-4-oxo-3-phenyl-3,4-dihydroquinazolin-2-yl)ethylcarbamate (1 g, 2.5 mmol) in dichloromethane (3 mL). The resultant was stirred at room temperature for 3 h. The solvents were removed in vacuo to afford the title compound as a white solid (823 mg). ES/MS *m/z* = 300.1 (M + H)⁺.

(S)-*tert*-Butyl 1-(5-Chloro-4-oxo-3-phenyl-3,4-dihydroquinazolin-2-yl)ethylcarbamate. Diphenyl phosphite (1.9 mL, 10 mmol) was added to a solution of 2-amino-6-chlorobenzoic acid (495 mg, 2.9 mmol) (**2**) and (*S*)-2-(*tert*-butoxycarbonylamino)propanoic acid (710 mg, 3.77 mmol) in pyridine (3 mL). The reaction mixture was stirred at 40 °C for 2 h. Aniline (274 mg, 3.48 mmol) was then added to the reaction mixture, which was then stirred at 55 °C for 12 h. The reaction mixture was cooled to room temperature. This mixture was then diluted with EtOAc (50 mL), washed with 1 N aqueous HCl (2 × 50 mL), brine (50 mL), and dried over sodium sulfate. The organics layer was filtered and concentrated in vacuo to afford material which was purified by column chromatography on SiO₂ eluting with EtOAc in hexanes (0–50%) to afford the title compound as a solid (1 g). ES/MS *m/z* = 400.1 (M + H)⁺.

2,4-Diamino-6-chloropyrimidine-5-carbonitrile. Ammonium hydroxide (20 mL) was added to a solution of 2,4,6-trichloropyrimidine-5-carbonitrile (5.0 g, 24 mmol) in dioxane (20 mL) at room temperature. The solution was warmed to 50 °C and stirred for 3 h. The reaction mixture was cooled to 10 °C, and water (50 mL) was added. The resulting solid was filtered, washed with water, and dried under high vacuum to afford the title compound as a white solid (4.5 g). ¹³C NMR (100 MHz, DMSO) 164.8, 162.6, 161.9, 115.8, 77.6. ES/MS *m/z* = 169.9 (M + H)⁺.

(S)-2-(1-((6-Amino-5-((5-fluoropyridin-2-yl)ethyl)pyrimidin-4-yl)amino)ethyl)-5-chloro-3-phenylquinazolin-4(3*H*)-one 2,2,2-Trifluoroacetate (31). **31** was synthesized according to the procedure described in [Scheme 2](#). To (*S*)-2-(1-aminoethyl)-5-chloro-3-phenylquinazolin-4(3*H*)-one 2,2,2-trifluoroacetic acid salt (58 mg, 0.14 mmol) and 6-chloro-5-((5-fluoropyridin-2-yl)ethyl)pyrimidin-4-amine (35 mg, 0.14 mmol) in IPA (2 mL) was added Hünig's base (0.14 mL, 0.7 mmol). The reagents were stirred at 130 °C for 14 h in a microwave reactor after which time the reaction mixture was cooled to room temperature. The solvent was evaporated and resultant solid was purified by HPLC eluting with 5–95% water/acetonitrile (0.1% v/v trifluoroacetic acid). The appropriate fractions were pooled and lyophilized to afford the title

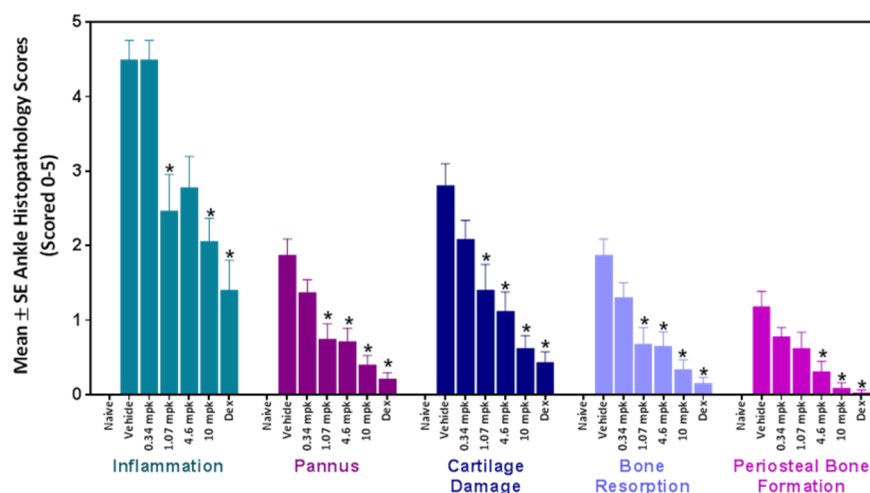


Figure 10. Analog **52** ameliorated histopathological disease severity in rats with established CIA. Ankle and knee joint tissue, sections from all animals were examined microscopically and graded on a scale from 0 to 5 for each parameter based on the degree of severity: (*) *p* < 0.05 versus arthritis + vehicle. See [Supporting Information](#) for scoring guidelines.

compound as a solid (32 mg). ^1H NMR (400 MHz, DMSO- d_6) δ 8.66 (d, J = 3.0 Hz, 1H), 7.88 (dd, J = 8.0, 4.0 Hz, 1H), 7.85–7.71 (m, 4H), 7.64–7.35 (m, 6H), 7.11 (d, J = 6.9 Hz, 1H), 6.83 (s, 2H), 4.67 (p, J = 6.5 Hz, 1H), 1.24 (d, J = 6.6 Hz, 3H). ES/MS m/z = 512.1 (M + H) $^+$.

6-Chloro-5-((5-fluoropyridin-2-yl)ethynyl)pyrimidin-4-amine. To 6-chloro-5-iodopyrimidin-4-amine (150 mg, 0.58 mmol) (in DMF (2 mL) were added Pd(PPh $_3$) $_2$ Cl $_2$ (28 mg, 0.04 mmol), CuI (5.5 mg, 0.029 mmol), TEA (2 mL), and 2-ethynyl-5-fluoropyridine (70 mg, 0.58 mmol). The reaction mixture was stirred at 90 °C for 2 h, after which time the reaction mixture was cooled to ambient temperature and partitioned between ethyl acetate (20 mL) and water (20 mL). The organic layer was washed with brine (25 mL), separated, dried over magnesium sulfate, and filtered. The resultant residue was purified on silica with 0–10% methanol in dichloromethane to afford the title compound as a solid (80 mg). ES/MS m/z = 249.3 (M + H) $^+$.

2-Ethynyl-5-fluoropyridine. To 5-fluoro-2-((trimethylsilyl)ethynyl)pyridine (400 mg, 2.06 mmol) in THF (5 mL) was added tetra-*n*-butylammonium fluoride (2.0 mL, 2.0 mmol). The reaction mixture was stirred at ambient temperature for 3 h, after which time the solvent was evaporated and the resultant residue was purified on silica gel with 0 to 100% ethyl acetate in hexanes to afford the title compound as an oil (150 mg). ES/MS m/z = 122.1 (M + H) $^+$.

5-Fluoro-2-((trimethylsilyl)ethynyl)pyridine. To 2-bromo-5-fluoropyridine (500 mg, 2.84 mmol) in THF (5 mL) were added Pd(PPh $_3$) $_2$ Cl $_2$ (136 mg, 0.19 mmol), CuI (26 mg, 0.13 mmol), TEA (5 mL), and ethynyltrimethylsilane (1.9 mL, 13.9 mmol). The reaction mixture was stirred at 70 °C for 2 h, after which time the solvent was evaporated. The resultant residue was purified on silica gel with 0–100% ethyl acetate in hexanes to afford the title compound as a solid (500 mg). ES/MS m/z = 226.3 (M + H) $^+$.

(S)-2-(1-((6-Aminopyrimidin-4-yl)amino)ethyl)-5-chloro-3-phenylquinazolin-4(3H)-one (15). The target compound was prepared in a manner analogous to that described for compound 34 as shown in Scheme 1. ^1H NMR (400 MHz, CDCl $_3$) δ 8.1 (s, 1), 7.7–7.3 (m, 8H), 5.63 (m, 1H), 5.35 (br s, 1H), 4.8 (m, 1H), 4.70 (br, 2H), 1.38 (d, 3H). ES/MS m/z 393.1 (M + H) $^+$.

(S)-5-Chloro-3-phenyl-2-(1-(pyrimidin-4-ylamino)ethyl)quinazolin-4(3H)-one (16). The target compound was prepared in a manner analogous to that described for compound 34 as shown in Scheme 1. ^1H NMR (400 MHz, DMSO- d_6) δ 9.85 (d, 1H), 8.75 (s, 1H), 8.2, (m, 1H), 7.8 (m, 1H), 7.7–7.4 (m, 7H), 6.8 (d, 1H), 4.70 (m, 1H), 1.4 (d, 3H). ES/MS m/z 378.1 (M + H) $^+$.

(S)-4-((1-(5-Chloro-4-oxo-3-phenyl-3,4-dihydroquinazolin-2-yl)ethyl)amino)pyrimidine-5-carbonitrile (17). The target compound was prepared in a manner analogous to that described for compound 34 as shown in Scheme 1. ^1H NMR (400 MHz, DMSO- d_6) δ 8.60 (bs, 1H), 8.51–8.46 (m, 2H), 7.83–7.74 (m, 1H), 7.66 (dd, J = 8.2, 1.2 Hz, 1H), 7.59 (dd, J = 7.8, 1.2 Hz, 1H), 7.57–7.52 (m, 1H), 7.52–7.46 (m, 1H), 7.46–7.41 (m, 1H), 7.40–7.30 (m, 2H), 4.90 (q, J = 6.7 Hz, 1H), 1.43 (d, J = 6.7 Hz, 3H). ES/MS m/z 403.1 (M + H) $^+$.

(S)-4-Amino-6-((1-(5-chloro-4-oxo-3-phenyl-3,4-dihydroquinazolin-2-yl)ethyl)amino)pyrimidine-5-carbonitrile (18) As Shown in Scheme 1. The target compound was prepared in a manner analogous to that described for compound 34. ^1H NMR (400 MHz, DMSO- d_6) δ 7.85 (s, 1H), 7.8–7.4 (m, 8H), 7.25 (br, 2H), 4.75 (m, 1H), 1.33 (d, 3H). ES/MS m/z 418.1 (M + H) $^+$.

(S)-2-Amino-4-((1-(5-chloro-4-oxo-3-phenyl-3,4-dihydroquinazolin-2-yl)ethyl)amino)nicotinonitrile (19). The target compound was prepared in a manner analogous to that described for compound 34 as shown in Scheme 1. ^1H NMR (400 MHz, DMSO- d_6) δ 7.80 (d, J = 7.9 Hz, 1H), 7.67 (d, J = 8.0 Hz, 1H), 7.60 (d, J = 7.7 Hz, 1H), 7.54 (s, 2H), 7.49–7.37 (m, 5H), 6.07 (s, 1H), 4.78–4.59 (m, 1H), 1.38 (s, 3H). ES/MS m/z 417.2 (M + H) $^+$.

(S)-2-Amino-4-((1-(5-chloro-4-oxo-3-phenyl-3,4-dihydroquinazolin-2-yl)ethyl)amino)pyrimidine-5-carbonitrile (20). The target compound was prepared in a manner analogous to that described for compound 34 as shown in Scheme 1. ^1H NMR (400 MHz, DMSO- d_6) δ 8.12 (s, 1H), 7.8 (d, 1H), 7.64 (dd, 1H), 7.58 (d,

1H), 7.36–7.56 (m, 5H), 6.9 (br, 3H), 4.8 (m, 1H), 1.35 (d, 3H). ES/MS m/z 418.1 (M + H) $^+$.

(S)-4-Amino-6-((1-(5-chloro-4-oxo-3-phenyl-3,4-dihydroquinazolin-2-yl)ethyl)amino)-2-hydroxypyrimidine-5-carbonitrile (21). To (S)-4-amino-6-((1-(5-chloro-4-oxo-3-phenyl-3,4-dihydroquinazolin-2-yl)ethyl)amino)-2-(methylsulfonyl)pyrimidine-5-carbonitrile (prepared as described for 33) in dioxane was added 1 M aqueous NaOH (10 equiv). The reaction mixture was allowed to stir at rt for 2 h. LCMS indicated consumption of starting material showing mostly desired sulfone and some sulfoxide. The material was extracted into EtOAc, concentrated to a residue which was taken up in DMSO, and purified by Prep HPLC. Clean fractions were pooled and lyophilized to give the desired product as a white powder (36% yield). ^1H NMR (400 MHz, DMSO- d_6) δ 7.82–7.75 (m, 1H), 7.75–7.69 (m, 2H), 7.63 (dd, J = 8.2, 1.2 Hz, 1H), 7.58 (dd, J = 7.8, 1.2 Hz, 1H), 7.56–7.33 (m, 3H), 4.62 (t, J = 6.7 Hz, 1H), 1.33 (d, J = 6.7 Hz, 3H). ES/MS m/z 434.1 (M + H) $^+$.

(S)-4-Amino-6-((1-(5-chloro-4-oxo-3-phenyl-3,4-dihydroquinazolin-2-yl)ethyl)amino)pyrimidine-5-carboxamide (22). The target compound was prepared in a manner analogous to that described for compound 34 as shown in Scheme 1. ^1H NMR (400 MHz, DMSO- d_6) δ 7.88 (d, 1H), 7.83 (s, 1H), 7.75 (t, 1H), 7.4–7.6 (m, 8H), 6.6 (br, 2H), 4.7 (m, 1H), 4.1 (br 1H), 3.3 (br 1H), 1.25 (d, 3H). ES/MS m/z 436.1 (M + H) $^+$.

(S)-2-(1-((6-Amino-5-(trifluoromethyl)pyrimidin-4-yl)amino)ethyl)-5-chloro-3-phenylquinazolin-4(3H)-one (23). The target compound was prepared in a manner analogous to that described for compound 34 as shown in Scheme 1. ^1H NMR (400 MHz, DMSO- d_6) δ 7.91 (s, 1H), 7.77 (t, 1H), 7.4–7.7 (m, 7H), 6.8 (br, 3H), 4.8 (m, 1H), 1.3 (d, 3H). ES/MS m/z 461.1 (M + H) $^+$.

(S)-2-(1-((6-Amino-5-methylpyrimidin-4-yl)amino)ethyl)-5-chloro-3-phenylquinazolin-4(3H)-one (24). The target compound was prepared in a manner analogous to that described for compound 34 as shown in Scheme 1. ^1H NMR (400 MHz, DMSO- d_6) δ 7.4–7.8 (m, 9H), 6.3 (d, 1H), 5.87 (br, 2H), 4.56 (m, 1H), 1.84 (s, 3H), 1.34 (d, 3H). ES/MS m/z 407.1 (M + H) $^+$.

(S)-2-(1-((6-Amino-5-methoxypyrimidin-4-yl)amino)ethyl)-5-chloro-3-phenylquinazolin-4(3H)-one (25). The target compound was prepared in a manner analogous to that described for compound 34 as shown in Scheme 1. ^1H NMR (400 MHz, DMSO- d_6) δ 8.00 (s, 1H), 7.77 (m, 1H), 7.65–7.54 (m, 2H), 7.52–7.43 (m, 2H), 7.40 (s, 3H), 4.73 (m, 1H), 3.65 (s, 3H), 1.49–1.31 (m, 3H). ES/MS m/z 423.1 (M + H) $^+$.

(S)-2-(1-((6-Amino-5-ethynylpyrimidin-4-yl)amino)ethyl)-5-chloro-3-phenylquinazolin-4(3H)-one (26). The target compound was prepared in a manner analogous to that described for compound 31 as shown in Scheme 2, using 12 and ethynyltrimethylsilane as the starting materials. ^1H NMR (400 MHz, DMSO- d_6) δ 7.82 (s, 1H), 7.76 (t, 1H), 7.4–7.7 (m, 7H), 6.7 (d, 1H), 6.54 (br, 2H), 4.77 (s, 1H), 4.7 (m, 1H), 1.3 (d, 3H). ES/MS m/z 417.1 (M + H) $^+$.

(S)-2-(1-(6-Amino-5-(phenylethynyl)pyrimidin-4-ylamino)ethyl)-5-chloro-3-phenylquinazolin-4(3H)-one (27). The target compound was prepared in a manner analogous to that described for compound 31 as shown in Scheme 2. ^1H NMR (400 MHz, DMSO- d_6) δ 7.88 (s, 1H), 7.78 (t, J = 8.0 Hz, 1H), 7.88 (dt, J = 6.8, 1.6 Hz, 2H), 7.59–7.41 (m, 10H), 6.92 (d, J = 7.0 Hz, 1H), 6.75 (br, 2H), 4.73 (p, J = 6.8 Hz, 1H), 1.35 (d, J = 6.7 Hz, 3H). ES/MS m/z 493.1 (M + H) $^+$.

(S)-2-(1-(6-Amino-5-(pyridin-3-ylethynyl)pyrimidin-4-ylamino)ethyl)-5-chloro-3-phenylquinazolin-4(3H)-one (28). The target compound was prepared in a manner analogous to that described for compound 31 as shown in Scheme 2. ^1H NMR (400 MHz, DMSO- d_6) δ 8.96 (d, J = 1.3 Hz, 1H), 8.62 (dd, J = 4.9, 1.7 Hz, 1H), 8.30–8.03 (m, 2H), 7.98 (s, 1H), 7.87–7.69 (m, 2H), 7.66–7.30 (m, 6H), 4.93–4.69 (m, 1H), 1.44 (d, J = 6.7 Hz, 3H). ES/MS m/z 494.1 (M + H) $^+$.

(S)-2-(1-(6-Amino-5-(pyrazin-2-ylethynyl)pyrimidin-4-ylamino)ethyl)-5-chloro-3-phenylquinazolin-4(3H)-one (29). The target compound was prepared in a manner analogous to that described for compound 31 as shown in Scheme 2. ^1H NMR (400 MHz, DMSO- d_6) δ 9.03 (d, J = 1.6 Hz, 1H), 8.78 (dd, J = 2.5, 1.6 Hz, 1H), 8.60 (d, J = 24.1 Hz, 1H), 8.07 (s, 1H), 7.92–7.68 (m, 2H),

7.64–7.23 (m, 9H), 4.89–4.61 (m, 1H), 1.34 (d, $J = 6.7$ Hz, 3H). ES/MS m/z 495.4 (M + H)⁺.

(S)-2-(1-(6-Amino-5-(pyridazin-3-ylethynyl)pyrimidin-4-ylamino)ethyl)-5-chloro-3-phenylquinazolin-4(3H)-one (30). The target compound was prepared in a manner analogous to that described for compound 31 as shown in Scheme 2. ¹H NMR (400 MHz, DMSO-*d*₆) δ 8.73 (d, $J = 2.9$ Hz, 1H), 8.01–7.79 (m, 4H), 7.73–7.39 (m, 8H), 7.38–7.17 (m, 2H), 4.85–4.74 (m, 1H), 1.35 (dd, $J = 13.1, 6.6$ Hz, 3H). ES/MS m/z 496.1 (M + H)⁺.

(S)-2-(1-(5-((1H-Pyrazol-4-yl)ethynyl)-6-aminopyrimidin-4-ylamino)ethyl)-5-chloro-3-phenylquinazolin-4(3H)-one (32). The target compound was prepared in a manner analogous to that described for compound 31 as shown in Scheme 2. ¹H NMR (400 MHz, DMSO-*d*₆) δ 8.11 (s, 1H), 8.01 (s, 2H), 7.76 (t, $J = 7.6$ Hz, 2H), 7.66–7.48 (m, 6H), 4.87–4.69 (m, 2H), 1.39 (d, $J = 6.5$ Hz, 3H). ES/MS m/z 483.1 (M + H)⁺.

(S)-4-Amino-6-((1-(5-chloro-4-oxo-3-phenyl-3,4-dihydroquinazolin-2-yl)ethyl)amino)pyrimidine-5-carbonitrile-2-d (33). To crude (S)-4-amino-6-((1-(5-chloro-4-oxo-3-phenyl-3,4-dihydroquinazolin-2-yl)ethyl)amino)-2-(methylsulfonyl)pyrimidine-5-carbonitrile in MeOD-*d*₄ (0.01M) was added NaBD₄ (2 equiv). The reaction mixture was allowed to stir overnight at rt. LCMS indicated consumption of starting material showing mostly desired deuterium incorporation as desired. The material was extracted into EtOAc, concentrated to a residue which was taken up in DMSO, and purified by Prep HPLC. Clean fractions were pooled and lyophilized to give the desired product as a white powder (40% yield). ¹H NMR (400 MHz, DMSO-*d*₆) δ 7.79 (td, $J = 8.0, 1.2$ Hz, 1H), 7.72–7.62 (m, 2H), 7.58 (dt, $J = 7.9, 1.3$ Hz, 1H), 7.55–7.29 (m, 5H), 4.78 (t, $J = 6.4$ Hz, 1H), 1.37 (dd, $J = 6.7, 1.1$ Hz, 3H). ES/MS m/z 419.1 (M + H)⁺.

(S)-4-Amino-6-((1-(5-chloro-4-oxo-3-phenyl-3,4-dihydroquinazolin-2-yl)ethyl)amino)-2-(methylsulfonyl)pyrimidine-5-carbonitrile. To (S)-4-amino-6-((1-(5-chloro-4-oxo-3-phenyl-3,4-dihydroquinazolin-2-yl)ethyl)amino)-2-(methylthio)pyrimidine-5-carbonitrile in THF (0.05M) were added MeOH (0.05 M) and water (0.05 M). Oxone (2 equiv) was added, and the reaction was allowed to stir overnight at rt. LCMS indicated consumption of starting material showing mostly desired sulfone and some sulfoxide. The crude material was extracted with EA, concentrated to an oil, and used crude in the next step.

(S)-4-Amino-6-((1-(5-chloro-4-oxo-3-phenyl-3,4-dihydroquinazolin-2-yl)ethyl)amino)-2-(methylthio)pyrimidine-5-carbonitrile. To (S)-4-chloro-6-((1-(5-chloro-4-oxo-3-phenyl-3,4-dihydroquinazolin-2-yl)ethyl)amino)-2-(methylthio)pyrimidine-5-carbonitrile is added ammonia in THF (13 equiv, 0.4 M). The reaction is heated at 75 °C and allowed to stir for 8 h. After cooling, hexanes were added to the reaction mixture and the solids were filtered to give the desired product as a white solid (70% yield).

(S)-4-Chloro-6-((1-(5-chloro-4-oxo-3-phenyl-3,4-dihydroquinazolin-2-yl)ethyl)amino)-2-(methylthio)pyrimidine-5-carbonitrile. To (S)-2-(1-aminoethyl)-5-chloro-3-phenylquinazolin-4(3H)-one in IPA (0.05M) were added 4,6-dichloro-2-(methylthio)pyrimidine-5-carbonitrile and DIEA (4 equiv). The reaction mixture was heated overnight at 75 °C. LCMS indicated good conversion to desired material. Hexanes were added to the reaction mixture, and the solids were filtered to result in the desired product as a white solid (82% yield).

(S)-4-Amino-2-chloro-6-((1-(5-chloro-4-oxo-3-phenyl-3,4-dihydroquinazolin-2-yl)ethyl)amino)pyrimidine-5-carbonitrile (35). The target compound was prepared in a manner analogous to that described for compound 34 as shown in Scheme 1. ¹H NMR (400 MHz, DMSO-*d*₆) δ 8.36 (d, $J = 6.7$ Hz, 2H), 7.91–7.27 (m, 9H), 4.50 (h, $J = 6.7$ Hz, 1H), 1.40–1.18 (m, 3H). ES/MS m/z 452.1 (M + H)⁺.

(S)-5-Chloro-2-(1-(2,6-diamino-5-chloropyrimidin-4-yl)-amino)ethyl-3-phenylquinazolin-4(3H)-one (36). The target compound was prepared in a manner analogous to that described for compound 34 as shown in Scheme 1 using 2,4-diamino-5-chloro-6-fluoropyrimidine as the starting material. ¹H NMR (400 MHz, DMSO-*d*₆) δ 7.80 (m, 1H), 7.71 (bs, 2H), 7.68 (dd, $J = 8.2, 1.2$ Hz, 1H), 7.60 (dd, $J = 7.8, 1.2$ Hz, 1H), 7.54–7.51 (m, 2H), 7.47 (bs, 2H),

7.43–7.40 (m, 3H), 7.32 (bs, 2H), 4.85 (p, $J = 6.7$ Hz, 1H), 1.36 (d, $J = 6.7$ Hz, 3H). ES/MS m/z 442.1 (M + H)⁺.

2,4-Diamino-5-chloro-6-fluoropyrimidine. To 2,4,6-trifluoropyrimidine (10 g, 75 mmol) in acetonitrile (100 mL) cooled to 0 °C was added conc NH₄OH (50 mL) in three portions. The reaction mixture was stirred at 40 °C for 12 h, after which time the reaction mixture was cooled to room temperature and concentrated in vacuo. The resulting solid was dissolved in MeOH/EtOH (250 mL, 1:1) and cooled to 0 °C. *N*-Chlorosuccinimide (13 g, 97 mmol) was added portionwise to the solution. The reaction mixture was stirred at 50 °C for 12 h, after which time the cooled reaction mixture was concentrated to approximately 150 mL in vacuo. The resultant suspension was cooled to –10 °C and the solid formed was collected by filtration and washed with water (100 mL) followed by 0.1 M NaOH (100 mL) and dried under high vacuum to afford the title compound as a white solid (8.7 g). ES/MS $m/z = 163.1$ (M + H)⁺.

(S)-2-Amino-4-chloro-6-((1-(5-chloro-4-oxo-3-phenyl-3,4-dihydroquinazolin-2-yl)ethyl)amino)pyrimidine-5-carbonitrile (37). The target compound was prepared in a manner analogous to that described for compound 34 as shown in Scheme 1. ¹H NMR (400 MHz, DMSO-*d*₆) δ 7.88–7.71 (m, 2H), 7.66 (dt, $J = 8.2, 1.0$ Hz, 1H), 7.59 (dt, $J = 7.8, 1.0$ Hz, 1H), 7.57–7.45 (m, 3H), 7.50–7.41 (m, 1H), 7.45–7.33 (m, 2H), 7.25 (s, 1H), 4.85 (q, $J = 6.7$ Hz, 1H), 1.36 (d, $J = 6.6$ Hz, 3H). ES/MS m/z 452.1 (M + H)⁺.

(S)-2-Amino-4-((1-(5-chloro-4-oxo-3-phenyl-3,4-dihydroquinazolin-2-yl)ethyl)amino)-6-methylpyrimidine-5-carbonitrile (38). The target compound was prepared in a manner analogous to that described for compound 34 as shown in Scheme 1. ¹H NMR (400 MHz, DMSO-*d*₆) δ 8.14 (s, 1H), 7.85–7.75 (m, 1H), 7.75–7.63 (m, 1H), 7.60 (dd, $J = 7.8, 1.4$ Hz, 1H), 7.54 (s, 2H), 7.55–7.46 (m, 2H), 7.47–7.33 (m, 3H), 4.94–4.83 (m, 1H), 2.35–2.29 (m, 3H), 1.37 (dt, $J = 6.7, 1.5$ Hz, 3H). ES/MS m/z 532.1 (M + H)⁺.

(S)-2,4-Diamino-6-((1-(5-chloro-3-(4-fluorophenyl)-4-oxo-3,4-dihydroquinazolin-2-yl)ethyl)amino)pyrimidine-5-carbonitrile (39). The target compound was prepared in a manner analogous to that described for compound 34 as shown in Scheme 1. ¹H NMR (400 MHz, DMSO-*d*₆) δ 7.90 (br, 1H), 7.8 (br, 1H), 7.78 (t, 1H), 7.65 (dd, $J = 8.2, 1.2$ Hz, 1H), 7.6 (m, 1H), 7.59 (dd, $J = 7.8, 1.2$ Hz, 1H), 7.44 (ddd, $J = 8.7, 5.0, 2.7$ Hz, 1H), 7.34 (td, $J = 8.7, 3.0$ Hz, 1H), 7.26 (td, $J = 8.7, 3.0$ Hz, 1H), 4.85 (m, 1H), 1.34 (d, $J = 6.6$ Hz, 3H). ES/MS m/z 451.1 (M + H)⁺.

(S)-2,4-dDiamino-6-((1-(5-chloro-3-(3-fluorophenyl)-4-oxo-3,4-dihydroquinazolin-2-yl)ethyl)amino)pyrimidine-5-carbonitrile (40). The target compound was prepared in a manner analogous to that described for compound 34 as shown in Scheme 1. ¹H NMR (400 MHz, DMSO-*d*₆) δ 8.0–7.75 (m, 4H), 7.80 (t, 1H), 7.67 (ddt, $J = 8.1, 2.9, 1.0$ Hz, 1H), 7.60 (d, 1H), 7.55–7.35 (m, 3H), 7.26 (m, 2H), 4.90 (dq, $J = 9.5, 6.7$ Hz, 1H), 1.36 (dd, $J = 6.8, 2.2$ Hz, 3H). ES/MS m/z 451.1 (M + H)⁺.

(S)-2,4-Diamino-6-(1-(5-chloro-3-(3-chlorophenyl)-4-oxo-3,4-dihydroquinazolin-2-yl)ethylamino)pyrimidine-5-carbonitrile (41). The target compound was prepared in a manner analogous to that described for compound 34 as shown in Scheme 1. ¹H NMR (400 MHz, DMSO-*d*₆) δ 7.79 (ddd, $J = 17.0, 10.3, 3.2$ Hz, 1H), 7.67 (ddd, $J = 13.3, 8.2, 1.2$ Hz, 1H), 7.60 (ddd, $J = 7.8, 4.6, 1.2$ Hz, 1H), 7.53–7.44 (m, 2H), 7.40 (qd, $J = 6.6, 4.6$ Hz, 1H), 5.00–4.83 (m, 1H), 1.36 (dd, $J = 9.4, 6.7$ Hz, 2H). ES/MS m/z 467.3 (M + H)⁺.

(S)-2,4-Diamino-6-(1-(5-chloro-3-(3-cyanophenyl)-4-oxo-3,4-dihydroquinazolin-2-yl)ethylamino)pyrimidine-5-carbonitrile (42). The target compound was prepared in a manner analogous to that described for compound 34 as shown in Scheme 1. ¹H NMR (400 MHz, DMSO-*d*₆) δ 8.13 (t, $J = 1.6$ Hz, 1H), 7.93 (ddd, $J = 8.0, 2.0, 1.2$ Hz, 1H), 7.88–7.83 (m, 1H), 7.80 (dd, $J = 9.5, 1.7$ Hz, 2H), 7.75–7.66 (m, 3H), 7.61 (ddd, $J = 7.5, 4.3, 3.2$ Hz, 1H), 7.18–7.08 (m, 1H), 6.77–6.68 (m, 1H), 4.96–4.77 (m, 1H), 1.33 (t, $J = 16.1$ Hz, 3H). ES/MS m/z 457.9 (M + H)⁺.

(S)-2,4-Diamino-6-((1-(5-chloro-3-(3-methoxyphenyl)-4-oxo-3,4-dihydroquinazolin-2-yl)ethyl)amino)pyrimidine-5-carbonitrile (43). The target compound was prepared in a manner analogous to that described for compound 34 as shown in Scheme 1. ¹H NMR

(400 MHz, DMSO- d_6) δ 7.82–6.85 (m, 7H), 5.01–4.90 (m, 1H), 3.74 (s, 3H), 1.35 (d, J = 6.6 Hz, 3H). ES/MS m/z 463.1 (M + H)⁺.

(S)-2,4-Diamino-6-(1-(5-chloro-4-oxo-3-(3-(trifluoromethyl)phenyl)-3,4-dihydroquinazolin-2-yl)ethylamino)pyrimidine-5-carbonitrile (44). The target compound was prepared in a manner analogous to that described for compound 34 as shown in Scheme 1. ¹H NMR (400 MHz, DMSO- d_6) δ 8.01 (d, J = 38.7 Hz, 1H), 7.91–7.75 (m, 3H), 7.75–7.63 (m, 4H), 7.63–7.52 (m, 2H), 5.02–4.74 (m, 1H), 1.43–1.19 (m, 3H). ES/MS 500.1 m/z (M + H)⁺.

(S)-2,4-Diamino-6-((1-(5-chloro-3-(3-(2,2-difluoroethyl)phenyl)-4-oxo-3,4-dihydroquinazolin-2-yl)ethylamino)pyrimidine-5-carbonitrile (45). The target compound was prepared in a manner analogous to that described for compound 34 as shown in Scheme 1. ¹H NMR (400 MHz, DMSO- d_6) δ 7.89–7.70 (m, 2H), 7.73–7.61 (m, 2H), 7.62–7.41 (m, 3H), 4.86 (dt, J = 57.5, 6.8 Hz, 1H), 1.93 (dt, J = 34.0, 18.9 Hz, 2H), 1.33 (dd, J = 13.4, 6.6 Hz, 3H). ES/MS 497.1 m/z (M + H)⁺.

(S)-2,4-Diamino-6-((1-(5-chloro-3-(3-(difluoromethyl)phenyl)-4-oxo-3,4-dihydroquinazolin-2-yl)ethylamino)pyrimidine-5-carbonitrile (46). The target compound was prepared in a manner analogous to that described for compound 34 as shown in Scheme 1. ¹H NMR (400 MHz, DMSO- d_6) δ 8.1–7.2 (m, 9H), 7.02 (m, 1H), 4.90 (m, 1H), 1.35 (m, 3H). ES/MS m/z 483.1 (M + H)⁺.

(S)-5-(5-Chloro-2-(1-((2,6-diamino-5-cyanopyrimidin-4-yl)amino)ethyl)-4-oxoquinazolin-3(4H)-yl)isophthalonitrile (47). The target compound was prepared in a manner analogous to that described for compound 34 as shown in Scheme 1. ¹H NMR (400 MHz, DMSO- d_6) δ 8.57–8.42 (m, 2H), 8.11 (q, J = 1.3 Hz, 1H), 7.86 (td, J = 8.0, 1.2 Hz, 1H), 7.74 (dt, J = 8.2, 1.2 Hz, 1H), 7.66 (dt, J = 7.8, 1.2 Hz, 1H), 4.90 (t, J = 6.8 Hz, 1H), 1.46–1.24 (m, 3H). ES/MS m/z 483.9 (M + H)⁺.

(S)-2,4-Diamino-6-(1-(5-chloro-3-(3-chloro-5-(difluoromethyl)phenyl)-4-oxo-3,4-dihydroquinazolin-2-yl)ethylamino)pyrimidine-5-carbonitrile (48). The target compound was prepared in a manner analogous to that described for compound 34 as shown in Scheme 1, using 3-chloro-5-(difluoromethyl)aniline as the starting material. ¹H NMR (400 MHz, DMSO- d_6) δ 7.96–7.75 (m, 3H), 7.72–7.64 (m, 2H), 7.63–7.50 (m, 4H), 7.21–6.78 (m, 3H), 4.97–4.87 (m, 1H), 1.39–1.31 (m, 3H). ES/MS m/z 517.1 (M + H)⁺.

3-Chloro-5-(difluoromethyl)aniline. A mixture of 1-chloro-3-(difluoromethyl)-5-nitrobenzene (980, 4.72 mmol) and 10% Pd/C (530 mg, 0.50 mmol) in ethyl acetate (20 mL) was stirred under an atmosphere of hydrogen for overnight. The reaction mixture was filtered over Celite followed by concentration to afford the title compound as a brown solid (578 mg).

1-Chloro-3-(difluoromethyl)-5-nitrobenzene. To a solution of 3-chloro-5-nitrobenzaldehyde (1.0 g, 5.38 mmol) in dichloromethane (30 mL) at 0 °C was added dropwise (diethylamino)sulfur trifluoride (1.42 mL, 10.8 mmol). The reaction mixture was stirred at room temperature for overnight. Water was slowly added, and the mixture was extracted twice with dichloromethane. The combined organic phases were washed with brine, dried over MgSO₄, filtered, and concentrated. The crude product was purified by silica gel column chromatography using 0–30% ethyl acetate in hexane to afford the title compound (980 mg).

(S)-2,4-Diamino-6-(1-(5-chloro-3-(3,5-difluorophenyl)-4-oxo-3,4-dihydroquinazolin-2-yl)ethylamino)pyrimidine-5-carbonitrile (49). The target compound was prepared in a manner analogous to that described for compound 34 as shown in Scheme 1. ¹H NMR (400 MHz, DMSO- d_6) δ 7.78 (t, J = 8.0 Hz, 1H), 7.65 (dd, J = 8.2, 1.2 Hz, 1H), 7.58 (dd, J = 7.8, 1.2 Hz, 1H), 7.43 (dm, J = 9.2 Hz, 1H), 7.29 (dt, J = 9.2, 2.4 Hz, 1H), 7.24 (dm, J = 11 Hz, 1H), 6.83 (d, J = 6.8 Hz, 1H), 6.51 (br s, 1H), 6.24 (br s, 1H), 4.82 (dq, J = 6.65, 6.65 Hz, 1H), 1.34 (d, J = 6.65 Hz, 3H). ES/MS m/z 469.1 (M + H)⁺.

(S)-2,4-Diamino-6-((1-(5-chloro-3-(3,5-difluorophenyl)-6-fluoro-4-oxo-3,4-dihydroquinazolin-2-yl)ethylamino)pyrimidine-5-carbonitrile (50). The target compound was prepared in a manner analogous to that described for compound 34 as shown in Scheme 1. ¹H NMR (400 MHz, DMSO- d_6) δ 8.01–7.72 (m, 7H), 7.49 (dm, J = 8.8 Hz, 1H), 7.34 (tt, J = 9.4, 2.4 Hz, 1H), 7.19–7.12

(m, 1H), 4.98 (p, J = 6.7 Hz, 1H), 1.40 (d, J = 6.6 Hz, 3H). ES/MS 487.1 m/z (M + H)⁺.

(S)-2,4-Diamino-6-(1-(3-(3,5-difluorophenyl)-4-oxo-3,4-dihydroquinazolin-2-yl)ethylamino)pyrimidine-5-carbonitrile (51). The target compound was prepared in a manner analogous to that described for compound 34 as shown in Scheme 1. ¹H NMR (400 MHz, DMSO- d_6) δ 8.32–8.10 (m, 1H), 7.91 (ddd, J = 23.8, 12.7, 9.1 Hz, 1H), 7.76 (dd, J = 14.1, 6.5 Hz, 1H), 7.68–7.56 (m, 1H), 7.50 (d, J = 9.2 Hz, 1H), 7.32 (tt, J = 9.3, 2.4 Hz, 1H), 7.18 (d, J = 9.1 Hz, 1H), 5.08–4.94 (m, 1H), 1.54–1.31 (m, 3H). ES/MS m/z 435.1 (M + H)⁺.

(S)-2,4-Diamino-6-(1-(3-(3,5-difluorophenyl)-5-fluoro-4-oxo-3,4-dihydroquinazolin-2-yl)ethylamino)pyrimidine-5-carbonitrile (52). The target compound was prepared in a manner analogous to that described for compound 34 as shown in Scheme 1. ¹H NMR (400 MHz, DMSO- d_6) δ 7.87 (dd, J = 13.6, 8.1 Hz, 1H), 7.57 (s, 2H), 7.55 (d, J = 8.2 Hz, 1H), 7.46 (d, J = 8.7 Hz, 1H), 7.38–7.19 (m, 2H), 7.15 (d, J = 8.6 Hz, 1H), 5.11–4.85 (m, 1H), 1.38 (d, J = 6.6 Hz, 3H). ES/MS m/z 453.3 (M + H)⁺.

(S)-2,4-Diamino-6-(1-(3-(3,5-difluorophenyl)-6-fluoro-4-oxo-3,4-dihydroquinazolin-2-yl)ethylamino)pyrimidine-5-carbonitrile (53). The target compound was prepared in a manner analogous to that described for compound 34 as shown in Scheme 1. ¹H NMR (400 MHz, DMSO- d_6) δ 7.88–7.67 (m, 4H), 7.48 (d, J = 9.1 Hz, 1H), 7.38–7.18 (m, 2H), 7.12 (d, J = 8.4 Hz, 2H), 5.11–4.88 (m, 1H), 1.34 (t, J = 37.5 Hz, 3H). ES/MS m/z 453.2 (M + H)⁺.

(S)-2,4-Diamino-6-(1-(3-(3,5-difluorophenyl)-8-fluoro-4-oxo-3,4-dihydroquinazolin-2-yl)ethylamino)pyrimidine-5-carbonitrile (54). The target compound was prepared in a manner analogous to that described for compound 34 as shown in Scheme 1. ¹H NMR (400 MHz, DMSO- d_6) δ 7.95 (d, J = 8.0 Hz, 2H), 7.86–7.69 (m, 2H), 7.58 (td, J = 8.0, 4.7 Hz, 2H), 7.48 (d, J = 9.0 Hz, 1H), 7.41–7.18 (m, 2H), 7.14 (d, J = 9.0 Hz, 1H), 5.09–4.86 (m, 1H), 1.40 (d, J = 6.6 Hz, 3H). ES/MS m/z 453.1 (M + H)⁺.

(S)-2-(1-((2,6-Diamino-5-cyanopyrimidin-4-yl)amino)ethyl)-3-(3,5-difluorophenyl)-4-oxo-3,4-dihydroquinazolin-8-carbonitrile (55). A mixture of (S)-2,4-diamino-6-((1-(3-(3,5-difluorophenyl)-8-iodo-4-oxo-3,4-dihydroquinazolin-2-yl)ethylamino)pyrimidine-5-carbonitrile (38 mg, 0.07 mmol) (synthesized in a manner analogous to Scheme 1) and copper(I) cyanide (1.5 equiv, 9 mg, 0.10 mmol) was taken up in *N*-methylpyrrolidinone (0.25 mL) in a 2–5 mL Smith process vial. The mixture was treated with tetrakis(triphenylphosphine)palladium(0) (10 mol %, 8 mg, 0.007 mmol) and irradiated for 1 h at 150 °C. The reaction mixture was partitioned between ethyl acetate and 10% aqueous hydrochloric acid. The insoluble brown material was removed by filtration. The aqueous phase was basified with concentrated ammonium hydroxide and was then extracted three times with ethyl acetate. The combined organics were washed once with saturated aqueous sodium chloride solution, dried over anhydrous magnesium sulfate, filtered, and concentrated under reduced pressure. The residue was purified by prep HPLC appropriate and fractions were combined and concentrated to afford the title compound (69 mg). ¹H NMR (400 MHz, DMSO- d_6) δ 8.46 (dd, J = 10.8, 1.6 Hz, 1H), 8.44 (dd, J = 11.2, 1.6 Hz, 1H), 7.87 (bs, 2H), 7.75 (t, J = 7.8 Hz, 1H), 7.74 (bs, 2H), 7.49 (m, 1H), 7.31 (tt, J = 9.3, 2.4 Hz, 1H), 7.06 (m, 1H), 5.14 (p, J = 6.6 Hz, 1H), 1.48 (d, J = 6.6 Hz, 3H). ES/MS m/z 460.1 (M + H)⁺.

PI3K Biochemical Assay. Enzymatic activity of the class I PI3K isoforms was measured using a time-resolved fluorescence resonance energy transfer (TR-FRET) assay that monitors formation of the product 3,4,5-inositol trisphosphate molecule (PIP3). Human full length p110 α and human p110 δ catalytic subunits were coexpressed with the p85 α regulatory subunit and purified as heterodimers. Human full length p110 γ was expressed and purified without a regulatory subunit. PI3K β was purchased from Millipore (Billerica, MA) (item 14-603, lot 1994929-B). All assay reagents and buffers for the TR-FRET assay were purchased from Millipore (Dundee, Ireland) (item 33-036, lot 1812413). PI3K isoforms were assayed under initial rate conditions at the following concentrations for each isoform: PI3K α , - β , - δ at 50 pM and PI3K γ at 5 nM. After an assay reaction time of 30 min at 25 °C, reactions were terminated with a final concentration of 10 mM EDTA, 10 nM labeled-PIP3, and 35 nM europium labeled GRP-1

detector protein before reading TR-FRET on an Envision plate reader (Ex, 340 nm; Em, 615/665 nm). Data were normalized based on a positive (1 μ M wortmannin) and negative (0.5% DMSO) control, and IC_{50} values were calculated from the fit of the dose–response curves to a four-parameter equation. All IC_{50} values represent geometric mean values of a minimum of four determinations.

EC₅₀, Whole Blood Basophil δ . Basophil activation was measured in human whole blood using the Flow2 CAST kit (Buhlmann Laboratories AG, Baselstrasse, Switzerland) following the protocol provided by the manufacturer with minor modifications. Human whole blood was collected into K2-EDTA venipuncture tubes. Whole blood samples were incubated with either DMSO (0.3% final) or a serial dilution of compounds in DMSO for 60 min at 37 °C. To activate basophils using the anti-Fc ϵ RI mAb; 50 μ L of whole blood was mixed with 130 μ L of stimulation buffer and 10 μ L of anti-Fc ϵ RI. Stimulation buffer alone was used as a negative control. The cells were stained with anti-CD63-FITC and anti-CCR3 (CD193)-PE antibodies for 25 min at 37 °C. Two mL lysis solution was added to lyse erythrocytes and to fix blood cells. After a 10 min incubation at room temperature, cells were pelleted and resuspended in wash buffer and analyzed by flow cytometry on a FCS00MPL flow cytometer (Beckman Coulter Inc., Fullerton, CA). Degranulation was detected via CD63 surface expression on CCR3 positive cells. The percent CD63 positive cells within the gated basophil population was determined in different treatment groups and normalized to the vehicle control (0.3% DMSO).

EC₅₀, B-Cell Activation Assay. The B-cell activation was measured in rat whole blood. Briefly, p110 δ was activated with BCR cross-linking with anti-IgD in the absence or presence of increasing concentrations of **52**. Whole blood was incubated with anti-IgD for 18–24 h to activate B-cells. To monitor the B-cell population and cellular activation in rats, anti-CD45RA-ECD (B-cell marker in Rats) and anti-CD86-PC5 (marker of B-cell activation in rats) antibodies were added to each sample. Flow cytometric analysis of the B-cell activation was performed on a FCS00MPL flow cytometer (Beckman Coulter Inc., Fullerton, CA). CD45RA-staining and side scatter were applied to gate at least 4000 B-cells that expressed a high density of CD45RA. The percentage of CD86 positive cells within the gated CD45RA+ B-cell population was determined in treatment groups and normalized to the vehicle control (0.3% DMSO). The final compound concentration was adjusted to correct for the dilution effect of added reagents. In this assay, the final serum concentration at the time of B-cell activation in rat whole blood was about 96%.

Microsome Stability Assay. Metabolic stability in vitro was determined using pooled hepatic microsomal fractions (final protein concentration of 0.5 mg/mL) at a final test compound concentration of 1 μ M. The reaction was initiated by the addition of an NADPH-regenerating system. An aliquot of 25 μ L of the reaction mixture was transferred at various time points to plates containing a quenching solution. The test compound concentration in the reaction mixture was determined with LC/MS/MS. Predicted clearance was calculated using the well-stirred liver model without protein restriction.

Hepatocyte Stability Assay. Metabolic stability in vitro was determined using human cryopreserved hepatocytes (1 \times 10⁶ viable cells/mL per well) at a final test compound concentration of 1 μ M in the presence or absence of raloxifene (5 μ M), a known inhibitor of aldehyde oxidase. An aliquot of 25 μ L of the reaction mixture was transferred at various time points to plates containing a quenching solution. The test compound concentration in the reaction mixture was determined with LC/MS/MS. Predicted clearance was calculated using the well-stirred liver model without protein restriction during incubation.

X-ray Crystallography. The crystallization and structure determination of PI3K δ bound with **32** and with **34** were determined using methods described previously.¹⁰ The PI3K δ /32 structure was refined to 2.85 Å resolution to an *R*-factor of 0.212 and an *R*_{free} of 0.306. The rms deviations from ideal bond distances and angles are 0.014 Å and 1.73°, respectively. The PI3K δ /34 structure was refined using data to 2.4 Å to an *R*-factor of 0.222 and an *R*_{free} of 0.290. The rms deviations

from ideal bond distances and angles are 0.010 Å and 1.31°, respectively.

DiscoverX Screen. Compound **52** was screened at 10 μ M in the KINOMEscan (DiscoverX, San Diego, CA) assay, and the results for the primary screen binding interactions are reported as “percent control”, where lower numbers indicate stronger hits in the matrix. See [Supporting Information](#) for assay results.

Pharmacokinetics. Pharmacokinetic studies for **52** were performed in female naive Lewis rats and non-naive beagle dogs (three animals per dosing route) following federal and Institutional Animal Care and Use Committee (IACUC) guidelines. Intravenous (iv) administration was dosed via infusion over 30 min. The intravenous dose for rats was formulated in a sterile solution of 30% PEG 400 (v/v) in water, while the intravenous dose for dogs was formulated in a sterile solution of 15% Captisol (w/v) in water. Oral dosing was administered by gavage. The oral dose for rats was formulated in a vehicle containing 30% PEG 400 (v/v) in water, while the oral dose for dogs was formulated in a vehicle of 5% ethanol, 55% PEG 400, and 40% citrate, pH 2. Blood samples were collected over a 24 h period postdose into Vacutainer tubes containing EDTA-K2. Plasma was isolated, and the concentration of the test compound in plasma was determined with LC/MS/MS after protein precipitation with acetonitrile. Noncompartmental pharmacokinetic analysis was performed on the plasma concentration–time data.

Rat-Collagen-Induced Arthritis (CIA) Model. The experiments were performed at Bolder BioPATH, Inc.^{20a,b} Female Lewis rats from Charles River (mean mass 180 g, (eight rats/group for arthritis, six rats/group for PK arm) were anesthetized with isoflurane and injected with 400 mL of Freund's incomplete adjuvant (Sigma-Aldrich) containing 2 mg/mL porcine type II collagen (Chondrex) at two sites (200 mL per site) at the base of the tail on day 0 and then 100 mL in one site at the base of the tail on day 7. On day 10 (day 1 of arthritis), rats were randomized into treatment groups such that each group had approximately equal mean ankle caliper measurements. Oral dosing was performed (twice daily at 12 h intervals) for 7 days (study days 10–16) with vehicle (30% PEG400/70% 10 mM, pH 2.2 citrate buffer), **52** (0.34, 1.07, 4.6, or 10 mg/kg), or the reference compound dexamethasone (Dex, 0.03 mg/kg). Rats were euthanized on days 16–17 (arthritis days 7–8). Rats were weighed on study days 9–17. Caliper measurements of right and left ankle diameters were taken every day beginning on day 9 (day 0 of arthritis) and continuing through day 16. Ankle caliper measurements were made with a Digitrix II micrometer (Fowler & NSK). Baseline measurements were taken using one ankle with values rounded to 1000th of an inch. Measurements were confirmed as clinically normal (0.260–0.264 in.) by comparison with historical values for rats based on a range of body weights. Baseline measurements were then applied to both ankles, and these values remained with the animal so long as the ankle was clinically normal with good definition of all the ankle bones and no evidence of inflammation. Body weight change and ankle diameter area under the curve (AUC) were calculated from dosing initiation through study termination (study days 10–16). Interim PK blood sampling was performed on study days 12 and 16 (arthritis days 3 and 7) at 2, 4, 8, and 12 h. Efficacy evaluation was based on animal body masses, daily ankle caliper measurements, ankle diameters expressed as the area under the curve (AUC), terminal hind paw masses, and histopathologic evaluation of ankles and knees.

■ ASSOCIATED CONTENT

📄 Supporting Information

The Supporting Information is available free of charge on the ACS Publications website at DOI: [10.1021/acs.jmedchem.6b00213](https://doi.org/10.1021/acs.jmedchem.6b00213).

Histopathology scoring criteria for rat CIA model, DiscoverX primary screen data and selectivity scores for **52** (PDF)

Molecular formula strings (CSV)

Accession Codes

PDB code for idelalisib is 4XE0. PDB code for compound 32 is S16U. PDB code for compound 34 is S14U.

AUTHOR INFORMATION

Corresponding Author

*Email: leena.patel@gilead.com. Phone: (206) 832-2058.

Present Addresses

J.E.: Acerta Pharma, 15400 SE 30th Place, Suite 206, Bellevue, WA 98007, U.S.

K.D.P.: Celgene Corporation, 10300 Campus Point Drive, Suite 100, San Diego, CA 92121, U.S.

Notes

The authors declare the following competing financial interest(s): The authors are employees of Gilead Sciences except for J.E. and K.D.P. who were employed at Gilead Sciences during this research. All authors are shareholders of Gilead Sciences.

ACKNOWLEDGMENTS

We thank Scott A. Mitchell and Jennifer Loyer-Drew for thoughtful review of the manuscript.

ABBREVIATIONS USED

PI3K, phosphoinositide 3-kinase; Akt, protein kinase B; BCR, B-cell receptor; RA, rheumatoid arthritis; HLM, human liver microsome; hHeps, human hepatocytes; AO, aldehyde oxidase; SAR, structure–activity relationship; CIA, collagen-induced arthritis; IgD, immunoglobulin D

REFERENCES

(1) (a) Engelman, J. A. Targeting PI3K signalling in cancer: opportunities, challenges and limitations. *Nat. Rev. Cancer* **2009**, *9* (8), 550–562. (b) Witzig, T. E.; Gupta, M. Signal transduction inhibitor therapy for lymphoma. *Hematology A. Soc. Hemato. Educ. Program* **2010**, *2010*, 265–270. (c) Lannutti, B. J.; Meadows, S. A.; Herman, S. E.; Kashishian, A.; Steiner, B.; Johnson, A. J.; Byrd, J. C.; Tyner, J. W.; Loriaux, M. M.; Deininger, M.; Druker, B. J.; Puri, K. D.; Ulrich, R. G.; Giese, N. A. CAL-101, a p110delta selective phosphatidylinositol-3-kinase inhibitor for the treatment of B-cell malignancies, inhibits PI3K signaling and cellular viability. *Blood* **2011**, *117* (2), 591–594. (d) Meadows, S. A.; Vega, F.; Kashishian, A.; Johnson, D.; Diehl, V.; Miller, L. L.; Younes, A.; Lannutti, B. J. PI3Kdelta inhibitor, GS-1101 (CAL-101), attenuates pathway signaling, induces apoptosis, and overcomes signals from the microenvironment in cellular models of Hodgkin lymphoma. *Blood* **2012**, *119* (8), 1897–1900.

(2) (a) Lemmon, M. A. Membrane recognition by phospholipid-binding domains. *Nat. Rev. Mol. Cell Biol.* **2008**, *9* (2), 99–111. (b) Bilancio, A.; Okkenhaug, K.; Camps, M.; Emery, J. L.; Ruckle, T.; Rommel, C.; Vanhaesebroeck, B. Key role of the p110delta isoform of PI3K in B-cell antigen and IL-4 receptor signaling: comparative analysis of genetic and pharmacologic interference with p110delta function in B cells. *Blood* **2006**, *107* (2), 642–650.

(3) Chantray, D.; Vojtek, A.; Kashishian, A.; Holtzman, D. A.; Wood, C.; Gray, P. W.; Cooper, J. A.; Hoekstra, M. F. p110δ, a novel phosphatidylinositol 3-kinase catalytic subunit that associates with p85 and is expressed predominantly in leukocytes. *J. Biol. Chem.* **1997**, *272* (31), 19236–19241.

(4) Bernal, A.; Pastore, R. D.; Asgary, Z.; Keller, S. A.; Cesarman, E.; Liou, H. C.; Schattner, E. J. Survival of leukemic B cells promoted by engagement of the antigen receptor. *Blood* **2001**, *98* (10), 3050–3057.

(5) Bartok, B.; Boyle, D. L.; Liu, Y.; Ren, P.; Ball, S. T.; Bugbee, W. D.; Rommel, C.; Firestein, G. S. PI3 kinase δ is a key regulator of synovial cell function in rheumatoid arthritis. *Am. J. Pathol.* **2012**, *180* (5), 1906–1916.

(6) Randis, T. M.; Puri, K. D.; Zhou, H.; Diacovo, T. G. Role of PI3Kδ and PI3Kγ in inflammatory arthritis and tissue localization of neutrophils. *Eur. J. Immunol.* **2008**, *38* (5), 1215–1224.

(7) Ali, K.; Bilancio, A.; Thomas, M.; Pearce, W.; Gilfillan, A. M.; Tkaczyk, C.; Kuehn, N.; Gray, A.; Giddings, J.; Peskett, E.; Fox, R.; Bruce, I.; Walker, C.; Sawyer, C.; Okkenhaug, K.; Finan, P.; Vanhaesebroeck, B. Essential role for the p110delta phosphoinositide 3-kinase in the allergic response. *Nature* **2004**, *431* (7011), 1007–1011.

(8) Puri, K. D.; Doggett, T. A.; Douangpanya, J.; Hou, Y.; Tino, W. T.; Wilson, T.; Graf, T.; Clayton, E.; Turner, M.; Hayflick, J. S.; Diacovo, T. G. Mechanisms and implications of phosphoinositide 3-kinase delta in promoting neutrophil trafficking into inflamed tissue. *Blood* **2004**, *103* (9), 3448–3456.

(9) Soond, D. R.; Bjorgo, E.; Moltu, K.; Dale, V. Q.; Patton, D. T.; Torgersen, K. M.; Galleway, F.; Twomey, B.; Clark, J.; Gaston, J. S.; Tasken, K.; Bunyard, P.; Okkenhaug, K. PI3K p110delta regulates T-cell cytokine production during primary and secondary immune responses in mice and humans. *Blood* **2010**, *115* (11), 2203–2213.

(10) Somoza, J. R.; Koditek, D.; Villasenor, A. G.; Novikov, N.; Wong, M. H.; Licican, A.; Xing, W.; Lagpacan, L.; Wang, R.; Schultz, B. E.; Papalia, G. A.; Samuel, D.; Lad, L.; McGrath, M. E. Structural, biochemical, and biophysical characterization of idelalisib binding to phosphoinositide 3-kinase δ. *J. Biol. Chem.* **2015**, *290* (13), 8439–8446.

(11) (a) Berndt, A.; Miller, S.; Williams, O.; Le, D. D.; Houseman, B. T.; Pacold, J. L.; Gorrec, F.; Hon, W.-C.; Liu, Y.; Rommel, C.; Gaillard, P.; Ruckle, T.; Schwarz, M. K.; Shokat, K. M.; Shaw, J. P.; Williams, R. L. The p110δ crystal structure uncovers mechanisms for selectivity and potency of novel PI3K inhibitors. *Nat. Chem. Biol.* **2010**, *6* (2), 117–124. (b) Knight, Z. A.; Gonzalez, B.; Feldman, M. E.; Zunder, E. R.; Goldenberg, D. D.; Williams, O.; Loewith, R.; Stokoe, D.; Balla, A.; Toth, B.; Balla, T.; Weiss, W. A.; Williams, R. L.; Shokat, K. M. A pharmacological map of the PI3-K family defines a role for p110α in insulin signaling. *Cell* **2006**, *125* (4), 733–747. (c) Knight, Z. A.; Shokat, K. M. Chemically targeting the PI3K family. *Biochem. Soc. Trans.* **2007**, *35* (2), 245–249.

(12) Flinn, I.; Horwitz, S.; Patel, M.; Younes, A.; Porter, J.; Sweeney, J.; Allen, K.; Kelly, P.; Kahl, B. Clinical safety and activity in a phase 1 trial of IPI-145, a potent inhibitor of phosphoinositide-3-kinase (δ/γ), in patients with advanced hematologic malignancies. *Blood (ASH Annual Meeting Abstracts)* **2012**, *120*, 3663.

(13) Cushing, T. D.; Hao, X.; Shin, Y.; Andrews, K.; Brown, M.; Cardozo, M.; Chen, Y.; Duquette, J.; Fisher, B.; Gonzalez-Lopez de Turiso, F.; He, X.; Henne, K. R.; Hu, Y.-L.; Hungate, R.; Johnson, M. G.; Kelly, R. C.; Lucas, B.; McCarter, J. D.; McGee, L. R.; Medina, J. C.; San Miguel, T.; Mohn, D.; Pattaropong, V.; Pettus, L. H.; Reichelt, A.; Rzas, R. M.; Seganish, J.; Tasker, A. S.; Wahl, R. C.; Wannberg, S.; Whittington, D. A.; Whoriskey, J.; Yu, G.; Zalameda, L.; Zhang, D.; Metz, D. P. Discovery and in Vivo Evaluation of (S)-N-(1-(7-Fluoro-2-(pyridin-2-yl)quinolin-3-yl)ethyl)-9H-purin-6-amine (AMG319) and Related PI3Kδ Inhibitors for Inflammation and Autoimmune Disease. *J. Med. Chem.* **2015**, *58* (1), 480–511.

(14) Currie, K. S. Targeting the B-cell receptor pathway in hematological malignancies. *Med. Chem. Rev.* **2015**, *50*, 230–231.

(15) Johnson, M.; Li, A.-R.; Liu, J.; Fu, Z.; Zhu, L.; Miao, S.; Wang, X.; Xu, Q.; Huang, A.; Marcus, A.; Xu, F.; Ebsworth, K.; Sablan, E.; Danao, J.; Kumer, J.; Dairaghi, D.; Lawrence, C.; Sullivan, T.; Tonn, G.; Schall, T.; Collins, T.; Medina, J. Discovery and optimization of a series of quinazolinone-derived antagonists of CXCR3. *Bioorg. Med. Chem. Lett.* **2007**, *17* (12), 3339–3343.

(16) (a) Jin, F.; Robeson, M.; Zhou, H.; Moyer, C.; Wilbert, S.; Murray, B.; Ramanathan, S. Clinical drug interaction profile of idelalisib in healthy subjects. *J. Clin. Pharmacol.* **2015**, *55* (8), 909–919. (b) Ramanathan, S.; Jin, F.; Sharma, S.; Kearney, B. P. Clinical pharmacokinetic and pharmacodynamic profile of idelalisib. *Clin. Pharmacokinet.* **2016**, *55*, 33–45.

(17) (a) Hall, W. W.; Krenitsky, T. A. Aldehyde oxidase from rabbit liver: specificity toward purines and their analogs. *Arch. Biochem.*

Biophys. **1986**, *251* (1), 36–46. (b) Torres, R. A.; Korzekwa, K. R.; McMaster, D. R.; Fandozzi, C. M.; Jones, J. P. Use of density functional calculations to predict the regioselectivity of drugs and molecules metabolized by aldehyde oxidase. *J. Med. Chem.* **2007**, *50* (19), 4642–4647. (c) Linton, A.; Kang, P.; Ornelas, M.; Kephart, S.; Hu, Q.; Pairish, M.; Jiang, Y.; Guo, C. Systematic structure modifications of imidazo[1,2-a]pyrimidine to reduce metabolism mediated by aldehyde oxidase (AO). *J. Med. Chem.* **2011**, *54* (21), 7705–7712. (d) Pryde, D. C.; Dalvie, D.; Hu, Q.; Jones, P.; Obach, R. S.; Tran, T.-D. Aldehyde oxidase: an enzyme of emerging importance in drug discovery. *J. Med. Chem.* **2010**, *53* (24), 8441–8460. (e) Rashidi, M.-R.; Pashaei-Asl, R. Role of aldehyde oxidase and xanthine oxidase in the metabolism of purine-related drugs. *Readings in Advanced Pharmacokinetics. Theory, Methods and Applications*, 1st ed.; Noreddin, A., Ed.; InTech: Rijeka, Croatia, 2012; pp 285–314, DOI: [10.5772/33202](https://doi.org/10.5772/33202).

(18) Zientek, M.; Jiang, Y.; Youdim, K.; Obach, R. S. In vitro-in vivo correlation for intrinsic clearance for drugs metabolized by human aldehyde oxidase. *Drug Metab. Dispos.* **2010**, *38* (8), 1322–1327.

(19) Pryde, D. C.; Tran, T.-D.; Jones, P.; Duckworth, J.; Howard, M.; Gardner, I.; Hyland, R.; Webster, R.; Wenham, T.; Bagal, S.; Omoto, K.; Schneider, R. P.; Lin, J. Medicinal chemistry approaches to avoid aldehyde oxidase metabolism. *Bioorg. Med. Chem. Lett.* **2012**, *22* (8), 2856–2860.

(20) (a) Bendele, A.; McComb, J.; Gould, T.; McAbee, T.; Sennello, G.; Chlipala, E.; Guy, M. Animal models of arthritis: relevance to human disease. *Toxicol. Pathol.* **1999**, *27* (1), 134–42. (b) Bendele, A. M. Animal models of rheumatoid arthritis. *J. Musculoskeletal Neuronal Interact.* **2001**, *1* (4), 377–385. (c) Trentham, D. E.; Townes, A. S.; Kang, A. H. Autoimmunity to type II collagen an experimental model of arthritis. *J. Exp. Med.* **1977**, *146* (3), 857–868.

■ NOTE ADDED AFTER ASAP PUBLICATION

After this paper was published ASAP on March 29, 2016, ref 13 was replaced. The corrected version was reposted April 5, 2016